Kernel signature space orthogonal projection for target detection in hyperspectral imagery

ZHAO Liaoying[1], ZHANG Kai[1], LI Xiaorun[2]

1. *Institute of Computer Application Technology, HangZhou Dianzi University, Zhejiang Hangzhou* 310018, *China*;
2. *College of Electrical Engineering, Zhejiang University, Zhejiang Hangzhou* 310027, *China*

Abstract: A kernel-based signature space orthogonal projection (KSSP) technique is proposed for nonlinear subpixel target detection in hyperspectral imagery. As a nonlinear version of the signature space orthogonal projection (SSP), the SSP is adopted in a high-dimension feature space after the pixels of input space are mapped into the feature space via nonlinear mapping. The kernel trick allows the KSSP ignor the actual nonlinear mapping. Experimental results of simulated and real data prove that the proposed KSSP approach outperforms the SSP method in target detection, and improves the robustness to noise.

Key words: signature space orthogonal projection, kernel function, subpixel target detection, kernel signature space orthogonal projection

CLC number: TP391 **Document code:** A

Citation format: Zhao L Y, Zhang K and Li X R. 2011. Kernel signature space orthogonal projection for target detection in hyperspectral imagery. *Journal of Remote Sensing*, 15(1): 13—28

1 INTRODUCTION

Object detection and identification by using hyperspectral image is a hot topic in the research area of remote sensing processing. Due to the limitation of spatial resolution and complexity of the ground objects, some interested objects can only be shown as subpixels, that is, each scene pixel in the image is generally mixed by the interested objects and the other ground objects. Subpixel target detection and identification is one of the critical key technologies for improving the utilization of hyperspectal.

In application, while the object and background spectral are known or obtained by some method beforehand, the spectral distribution (abundant) of object and background is usually computed approximately to estimate whether the object exists or not. Recently, several algorithms have been investigated, which include least squares, orthogonal subspace projection approach (OSP), and signature space orthogonal projection (SSP) (Chang, *et al.*, 1998). But all these methods are proposed based on linear spectrum mixture model.

Spectral mixing can be essentially classified into the linear spectrum mixture model and the nonlinear spectrum mixture model. The linear spectrum mixture model has the advantages of simple structure with specific physical signification, and has more scientific in theory. However, a linear spectrum mixture model is mostly applied when ground object is basically or mostly linear mixed or can be viewed as linear mixed in macroscopic scale. The nonlinear mixture model is required for the fine spectral analysis in microscopic scale or for the detection of object with small probability. Some typical models used nowadays are Hapke model, Kubelk-Munk model, vegetation & soil mixed model based on radiation flux density theory and SAIL model (Tong, *et al*, 2006). However, each of them has its own appliable field and limitation. Furthermore, it is very hard to build the nonlinear mixture model.

With the successful application of support vector machine (SVM) in various research fields, it is popular in machine-based learning that linear methods is expected to solve the nonlinear problems by using kernel function. Kernel-based learning methods are a kind of efficient nonlinear data analysis method which can avoid making sure the nonlinear relationship and computing nonlinear model (Shawe-Taylor, *et al.*, 2005). Nowadays, kernel-based methods have been widely used in hyperspectral images classification and object detection. Particularly, Kwon (2005) who worked in the America Army Research Lab has extended the subspace-matched detector (MSD), orthogonal subspace detector (OSD), spectral-matched filter (SMF) and adaptive subspace detectors (ASD) to the kernel-matched subspace detector (KMSD), the kernel orthogonal subspace detector (KOSD), the kernel spectral-matched filter (KSMF), and the kernel adaptive subspace detectors (KASD) respectively. In addition, Capobianco, *et al.* (2008) presented contextual versions of the KOSP.

SSP is a posteriori KOSP proposed by Chang, et al. (1998)

Received: 2009-12-21; **Accepted**: 2010-04-22

Foundation: The Zhejiang Natural science Foundation (No. Y1100196).

First author biography: ZHAO Liaoying(1970—), female, associated professor, Ph.D.. Her research interest focuses on pattern recognition and remote sense image analysis. E-mail: zhaoly@hdu.edu.cn

based on the least squares. Based on the ideas of SSP and kernel-based learning theory, a kernel version of the SSP also called kernel signature orthogonal space projection (KSSP) is proposed In this paper, which maps the pixels of input space into the high-dimension feature space so as to satisfy the linear mixture modal. Then, the object detection will be fulfilled by using the SSP algorithm in the feature space. In order to evaluate the performance of the SSP and KSSP, we model their associated least squares errors as a signal detection problem in the framework of the N-P(Neyman-Pearson)theory. The effectiveness of the two algorithms can be measured by using the ROC (Receiver Operating Characteristic Curve)analysis. Experimental results of both simulated and real data demonstrate that the proposed KSSP approach outperforms the SSP method in the target detection of nonlinear-mixed hyperspectral image, and improves robustness to noise.

2 SIGNATURE SPACE ORTHOGONAL PROJECTION

Let $\boldsymbol{r}$ be a $L\times1$ column vector representing the observation spectrum and $\boldsymbol{M}$ be a $L\times p$ matrix whose columns are the endmember spectra. Let α is a $p\times1$ column vector whose elements are the coefficients that account for the proportions (abundances) of each endmember spectrum contributing to the mixed pixel and n is a $L\times1$ vector representing an additive noise. The linear mixture model (LSMM) for pixel $\boldsymbol{r}$ is described by Eq.(1).

$$\boldsymbol{r}=\boldsymbol{M}\boldsymbol{\alpha}+\boldsymbol{n} \tag{1}$$

The OSP algorithm assumes that each pixel is made up of a designed signature $\boldsymbol{d}=\boldsymbol{m}_i$, $1\leqslant i\leqslant p$ and the undersigned background signature matrix $\boldsymbol{U}=(\boldsymbol{m}_1,\cdots,\boldsymbol{m}_{i-1},\boldsymbol{m}_{i+1},\cdots,\boldsymbol{m}_p)$. Then Eq.(1) can be rewritten as follows.

$$\boldsymbol{r}=\boldsymbol{d}\alpha_i+\boldsymbol{U}\gamma+\boldsymbol{n} \tag{2}$$

where α_i is the fraction of $\boldsymbol{m}_i$ in the pixel $\boldsymbol{r}$ and $\gamma=(\alpha_1,\cdots,\alpha_{i-1},\alpha_{i+1},\cdots,\alpha_p)^{\mathrm{T}}$ is the corresponding abundance column vector of the background signatures.

The OSP algorithm is obtained by maximizing SNR under the assumption that the complete knowledge of signature abundance a priori, which is generally difficult to obtain in practice. Under the circumstance, we must estimate the signatures from the data themselves. The SSP use the posteriori model as follows.

$$\boldsymbol{r}=\boldsymbol{M}\hat{\boldsymbol{\alpha}}+\hat{\boldsymbol{n}}=\boldsymbol{d}\hat{\alpha}_i+\boldsymbol{U}\hat{\gamma}+\hat{\boldsymbol{n}} \tag{3}$$

where $\hat{\boldsymbol{\alpha}},\hat{\alpha}_i$ and $\hat{\gamma}$ are estimates of $\boldsymbol{\alpha}$, α_i and γ, respectively, based on the observed pixel $\boldsymbol{r}$ itself.

Fig.1 shows the sketch map of the SSP approach, where $\boldsymbol{P}_{\boldsymbol{M}}=\boldsymbol{M}(\boldsymbol{M}^{\mathrm{T}}\boldsymbol{M})^{-1}\boldsymbol{M}^{\mathrm{T}}$ is the signature space orthogonal projector and $\boldsymbol{P}_{\boldsymbol{U}}^{\perp}=\boldsymbol{I}-\boldsymbol{U}(\boldsymbol{U}^{\mathrm{T}}\boldsymbol{U})^{-1}\boldsymbol{U}^{\mathrm{T}}$ denotes the background rejection operator.

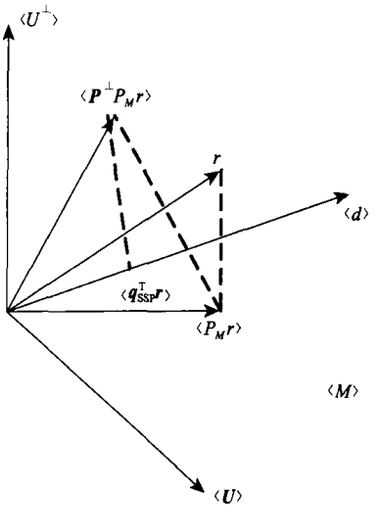

Fig.1 Signature space orthogonal projection

The SSP operator is given by Eq.(4).

$$\boldsymbol{q}_{\mathrm{SSP}}^{\mathrm{T}}=\boldsymbol{d}^{\mathrm{T}}\boldsymbol{p}_{\boldsymbol{U}}^{\perp}\boldsymbol{P}_{\boldsymbol{M}} \tag{4}$$

and the normalized SSP operator can be defined by Eq.(5).

$$\tilde{\boldsymbol{q}}_{\mathrm{SSP}}^{\mathrm{T}}=\frac{\boldsymbol{q}_{\mathrm{SSP}}^{\mathrm{T}}}{\boldsymbol{d}^{\mathrm{T}}\boldsymbol{P}_{\boldsymbol{U}}^{\perp}\boldsymbol{P}_{\boldsymbol{M}}\boldsymbol{d}}=\frac{\boldsymbol{q}_{\mathrm{SSP}}^{\mathrm{T}}}{\boldsymbol{d}^{\mathrm{T}}\boldsymbol{P}_{\boldsymbol{U}}^{\perp}\boldsymbol{d}} \tag{5}$$

where the last equality holds because of $\boldsymbol{d}^{\mathrm{T}}\boldsymbol{P}_{\boldsymbol{U}}^{\perp}\boldsymbol{d}=\boldsymbol{d}^{\mathrm{T}}\boldsymbol{P}_{\boldsymbol{U}}^{\perp}\boldsymbol{P}_{\boldsymbol{M}}\boldsymbol{d}$. The output of the SSP classifier is now given by Eq.(6).

$$\boldsymbol{D}_{\mathrm{SSP}}(\boldsymbol{r})=\tilde{\boldsymbol{q}}_{\mathrm{SSP}}^{\mathrm{T}}\boldsymbol{r}=\frac{\boldsymbol{d}^{\mathrm{T}}\boldsymbol{P}_{\boldsymbol{U}}^{\perp}\boldsymbol{P}_{\boldsymbol{M}}\boldsymbol{r}}{\boldsymbol{d}^{\mathrm{T}}\boldsymbol{P}_{\boldsymbol{U}}^{\perp}\boldsymbol{d}} \tag{6}$$

Applying $\tilde{\boldsymbol{q}}_{\mathrm{SSP}}^{\mathrm{T}}$ to both a priori model (4) and a posteriori model (5), the estimation error is given by Eq.(7).

$$\varepsilon=\hat{\alpha}_i-\boldsymbol{D}_{\mathrm{SSP}}=\tilde{\boldsymbol{q}}_{\mathrm{SSP}}^{\mathrm{T}}\boldsymbol{n}=\frac{\boldsymbol{d}^{\mathrm{T}}\boldsymbol{P}_{\boldsymbol{U}}^{\perp}\boldsymbol{P}_{\boldsymbol{M}}\boldsymbol{n}}{\boldsymbol{d}^{\mathrm{T}}\boldsymbol{P}_{\boldsymbol{U}}^{\perp}\boldsymbol{d}} \tag{7}$$

with the corresponding $\mathrm{SNR}_{\mathrm{SSP,max}}$ given by the maximum eigenvalue (Chang, *et al.*, 1998) as follows.

$$\lambda_{\mathrm{SSP,max}}=\frac{\alpha_i^2}{\sigma^2}\boldsymbol{d}^{\mathrm{T}}\boldsymbol{P}_{\boldsymbol{U}}^{\perp}\boldsymbol{d} \tag{8}$$

where σ is the noise root variance.

If $\boldsymbol{d}$ is very similar to one or more signatures in $\boldsymbol{U}$, the normalization coefficient $\boldsymbol{d}^{\mathrm{T}}\boldsymbol{P}_{\boldsymbol{U}}^{\perp}\boldsymbol{d}$ will be small, and so will be the SNR. Therefore, the magnitude of $\boldsymbol{d}^{\mathrm{T}}\boldsymbol{P}_{\boldsymbol{U}}^{\perp}\boldsymbol{d}$ can be used as a measure of the target signature discrimination power of SSP. The larger the $\boldsymbol{d}^{\mathrm{T}}\boldsymbol{P}_{\boldsymbol{U}}^{\perp}\boldsymbol{d}$ is, the better the discrimination.

3 KERNEL SIGNATURE SPACE ORTHGONAL PROJECTION

3.1 LSMM and SSP in feature space

Linear mixing is a kind of special nonlinear mixing which the multiple reflections can be ignored. Assuming that the input data has been implicitly mapped into a high-dimensional

feature space H by a nonlinear mapping ϕ, the mixture model in feature space is approximately linear if the multiple reflections of all pixels in H is small. Let $\boldsymbol{M}_\phi$ be a matrix whose columns are the endmember spectra in the feature space; $\boldsymbol{\alpha}$ be a coefficient vector that account for the abundance of each endmember spectrum in the feature space; and $\boldsymbol{n}_\phi$ be an additive noise, the linear mixture model in feature space is given by the following equation.

$$\phi(\boldsymbol{r}) = \boldsymbol{M}_\phi \boldsymbol{\alpha} + \boldsymbol{n}_\phi \tag{9}$$

Corresponding to Eq.2, the model (9) can also be further rewritten as follows.

$$\phi(\boldsymbol{r}) = \phi(\boldsymbol{d})\alpha_i + \boldsymbol{U}_\phi \boldsymbol{\gamma} + \boldsymbol{n}_\phi \tag{10}$$

where $\phi(\boldsymbol{d})$ represents the spectral signature of the desired target with the corresponding abundance α_i in the feature space and the column of $\boldsymbol{U}_\phi$ represents the undesired background signatures in the feature space with the related abundance $\boldsymbol{\gamma}$.

The normalize SSP operator of pixel $\boldsymbol{r}$ in the feature space can easily be derived by using the same procedure for the conventional SSP operator Eq.(5) and Eq.(6). The normalize SSP operator in the feature space is given by Eq.(11) and Eq.(12).

$$\tilde{q}_{\mathrm{SSP}\phi}^{\mathrm{T}} = \frac{\phi(\boldsymbol{d})^{\mathrm{T}} \boldsymbol{P}_{U_\phi}^{\perp} \boldsymbol{P}_{M_\phi}}{\phi(\boldsymbol{d})^{\mathrm{T}} \boldsymbol{P}_{U_\phi}^{\perp} \phi(\boldsymbol{d})} \tag{11}$$

$$D_{\mathrm{SSP}\phi}(\boldsymbol{r}) = \frac{\phi(\boldsymbol{d}) \boldsymbol{P}_{U_\phi}^{\perp} \boldsymbol{P}_{M_\phi} \phi(\boldsymbol{r})}{\phi(\boldsymbol{d})^{\mathrm{T}} \boldsymbol{P}_{U_\phi}^{\perp} \phi(\boldsymbol{d})} \tag{12}$$

where $\boldsymbol{P}_{M_\phi} = \boldsymbol{M}_\phi (\boldsymbol{M}_\phi^{\mathrm{T}} \boldsymbol{M}_\phi)^{-1} \boldsymbol{M}_\phi^{\mathrm{T}}$, $\boldsymbol{P}_{U_\phi}^{\perp} = \boldsymbol{I}_\phi - \boldsymbol{U}_\phi \boldsymbol{U}_\phi^{\#} = \boldsymbol{I}_\phi - \boldsymbol{U}_\phi (\boldsymbol{U}_\phi^{\mathrm{T}} \boldsymbol{U}_\phi)^{-1} \boldsymbol{U}_\phi^{\mathrm{T}}$, and $\boldsymbol{I}_\phi$ is the identity matrix in the feature space.

Similarly, the estimation error of abundance is given by Eq.(13).

$$\varepsilon = \frac{\phi(\boldsymbol{d}) \boldsymbol{P}_{U_\phi}^{\perp} \boldsymbol{P}_{M_\phi} \boldsymbol{n}_\phi}{\phi(\boldsymbol{d})^{\mathrm{T}} \boldsymbol{P}_{U_\phi}^{\perp} \phi(\boldsymbol{d})} \tag{13}$$

with the corresponding maximum SNR as follows.

$$\mathrm{SNR}_{\mathrm{SSP}\phi,\max} = \frac{\alpha_i^2}{\theta^2} \phi(\boldsymbol{d})^{\mathrm{T}} \boldsymbol{P}_{U_\phi}^{\perp} \phi(\boldsymbol{d}) \tag{14}$$

where θ is the noise root variance in the feature space.

Due to the difficulty to confirm an actual nonlinear mapping ϕ, Eq.(11)–Eq.(14) are not able to directly implement. However, it can be implemented by employing kernel functions using an efficient kernel trick without any knowledge of the actual nonlinear mapping ϕ.

3.2 KSSP algorithm

In this section, we demonstrate how to kernelize the SSP in the feature space by kernel trick, and the corresponding algorithm is called kernel signature space orthogonal projection (KSSP). The definition of the kernel function is given as follows.

Definition 1 (Kernel function) A kernel is a function k that for all $\boldsymbol{x}, \boldsymbol{z} \in \boldsymbol{X}$, $\boldsymbol{X} \subset \boldsymbol{R}^n$ satisfies

$$k(\boldsymbol{x}, \boldsymbol{z}) = \langle \phi(\boldsymbol{x}) \cdot \phi(\boldsymbol{z}) \rangle \tag{15}$$

where ϕ is a nonlinear map from input space $\boldsymbol{X}$ to a dot production feature space $\boldsymbol{H}$, and $\langle \cdot \rangle$ is the dot products.

Any function satisfied Mercer theorem or the positive property can be used as a kernel function (Shawe-Taylor, *et al.*, 2005). Some commonly-used kernel functions include radial basis function (RBF) kernel: $k(\boldsymbol{x}, \boldsymbol{z}) = \exp\left(-\frac{\|\boldsymbol{x} - \boldsymbol{z}\|^2}{2\sigma^2}\right)$, where σ is the kernel parameter, and the polynomial kernel function: $k(\boldsymbol{x}, \boldsymbol{z}) = (a\boldsymbol{x}^{\mathrm{T}}\boldsymbol{z} + c)^b$, where a, b, c are parameters.

According to the definition of kernel function, each element in matrix $\boldsymbol{K}_{UU} = \boldsymbol{U}_\phi^{\mathrm{T}} \boldsymbol{U}_\phi$ and $\boldsymbol{K}_{MM} = \boldsymbol{M}_\phi^{\mathrm{T}} \boldsymbol{M}_\phi$ is a kernel function, and the matrix $\boldsymbol{K}_{UU}$ and $\boldsymbol{K}_{MM}$ are the kernel matrixes.

In order to express Eq.(12) as an kernel function expression, we analyze the matrix $\boldsymbol{K}_{UU}$ and $\boldsymbol{K}_{MM}$ in detail.

Suppose the rank of matrix $\boldsymbol{U}_\phi^{\mathrm{T}} \boldsymbol{U}_\phi$ is N_b, $\lambda_i (i = 1, 2, \cdots, N_b)$ are the nonzero eigenvalues of matrix $\boldsymbol{U}_\phi^{\mathrm{T}} \boldsymbol{U}_\phi$, $\boldsymbol{\Sigma}_\phi = diag(\lambda_1, \lambda_2, \cdots, \lambda_{N_b})$, and $\boldsymbol{A}_\phi = [\boldsymbol{a}_\phi^1, \boldsymbol{a}_\phi^2, \cdots, \boldsymbol{a}_\phi^{N_b}]$ is the eigenvector matrix of $\boldsymbol{U}_\phi^{\mathrm{T}} \boldsymbol{U}_\phi$ corresponding to $\boldsymbol{\Sigma}_\phi$, then using the singular value decomposition theorem and its deduction (Zhaoqi Bian, *et al.*, 2000), we get

$$\boldsymbol{U}_\phi^{\mathrm{T}} \boldsymbol{U}_\phi = \boldsymbol{A}_\phi \boldsymbol{\Sigma}_\phi \boldsymbol{A}_\phi^{\mathrm{T}} \tag{16}$$

therefore,

$$\boldsymbol{P}_{U_\phi} = \boldsymbol{U}_\phi \boldsymbol{A}_\phi \boldsymbol{\Sigma}_\phi^{-1} \boldsymbol{A}_\phi^{\mathrm{T}} \boldsymbol{U}_\phi^{\mathrm{T}} \tag{17}$$

$$\boldsymbol{P}_{U_\phi}^{\perp} = \boldsymbol{I}_\phi - \boldsymbol{U}_\phi \boldsymbol{A}_\phi \boldsymbol{\Sigma}_\phi^{-1} \boldsymbol{A}_\phi^{\mathrm{T}} \boldsymbol{U}_\phi^{\mathrm{T}} \tag{18}$$

Similarly, suppose the rank of matrix $\boldsymbol{M}_\phi^{\mathrm{T}} \boldsymbol{M}_\phi$ is t, υ_i is the nonzero eigenvalues of $\boldsymbol{M}_\phi^{\mathrm{T}} \boldsymbol{M}_\phi$, $\boldsymbol{\Sigma}_{M\phi} = diag(\upsilon_1, \upsilon_2, \cdots, \upsilon_t)$, and $\boldsymbol{X}_\phi$ is the eigenvector of $\boldsymbol{M}_\phi^{\mathrm{T}} \boldsymbol{M}_\phi$ corresponding to $\boldsymbol{X}_\phi$, then

$$\boldsymbol{M}_\phi^{\mathrm{T}} \boldsymbol{M}_\phi = \boldsymbol{X}_\phi \boldsymbol{\Sigma}_{M\phi} \boldsymbol{X}_\phi^{\mathrm{T}} \tag{19}$$

therefore,

$$\boldsymbol{P}_{M_\phi} = \boldsymbol{M}_\phi \boldsymbol{X}_\phi \boldsymbol{\Sigma}_{M\phi}^{-1} \boldsymbol{X}_\phi^{\mathrm{T}} \boldsymbol{M}_\phi^{\mathrm{T}} \tag{20}$$

Substituting Eq.(18) and Eq.(20) into Eq.(12) results in the following equation.

$$D_{\mathrm{SSP}\phi}(\boldsymbol{r}) = \frac{\phi(\boldsymbol{d})^{\mathrm{T}} \boldsymbol{M}_\phi \boldsymbol{X}_\phi \boldsymbol{\Sigma}_{M_\phi}^{-1} \boldsymbol{X}_\phi^{\mathrm{T}} \boldsymbol{M}_\phi^{\mathrm{T}} \phi(\boldsymbol{r}) - \phi(\boldsymbol{d})^{\mathrm{T}} \boldsymbol{U}_\phi \boldsymbol{A}_\phi \boldsymbol{\Sigma}_\phi^{-1} \boldsymbol{A}_\phi^{\mathrm{T}} \boldsymbol{U}_\phi^{\mathrm{T}} \boldsymbol{M}_\phi \boldsymbol{X}_\phi \boldsymbol{\Sigma}_{M_\phi}^{-1} \boldsymbol{X}_\phi^{\mathrm{T}} \boldsymbol{M}_\phi^{\mathrm{T}} \phi(\boldsymbol{r})}{\phi(\boldsymbol{d})^{\mathrm{T}} \phi(\boldsymbol{d}) - \phi(\boldsymbol{d})^{\mathrm{T}} \boldsymbol{U}_\phi \boldsymbol{A}_\phi \boldsymbol{\Sigma}_\phi^{-1} \boldsymbol{A}_\phi^{\mathrm{T}} \boldsymbol{U}_\phi^{\mathrm{T}} \phi(\boldsymbol{d})} \tag{21}$$

Similarly, each element of vectors $\phi(\boldsymbol{d})^{\mathrm{T}}\boldsymbol{M}_{\phi}$, $\boldsymbol{M}_{\phi}{}^{\mathrm{T}}\phi(\boldsymbol{r})$, $\phi(\boldsymbol{d})^{\mathrm{T}}\boldsymbol{U}_{\phi}$ and $\boldsymbol{U}_{\phi}^{\mathrm{T}}\phi(\boldsymbol{d})$ is also a kernel function, denote these vectors as $\boldsymbol{K}_{dM}$, $\boldsymbol{K}_{Mr}$, $\boldsymbol{K}_{dU}$ and $\boldsymbol{K}_{Ud}$ respectively, each element of matrix $\boldsymbol{U}_{\phi}^{\mathrm{T}}\boldsymbol{M}_{\phi}$, which can be denoted as $\boldsymbol{K}_{UM}$, is also a kernel function, $k_{dd}=\phi(\boldsymbol{d})^{\mathrm{T}}\phi(\boldsymbol{d})$ is a kernel function too. Then, Eq.(21) can be simply rewritten as:

$$D_{\mathrm{KSSP}}(\boldsymbol{r})=\frac{\boldsymbol{K}_{dM}\boldsymbol{X}_{\phi}\boldsymbol{\Sigma}_{M_{\phi}}^{-1}\boldsymbol{X}_{\phi}{}^{\mathrm{T}}\boldsymbol{K}_{Mr}-\boldsymbol{K}_{dU}\boldsymbol{A}_{\phi}\boldsymbol{\Sigma}_{\phi}^{-1}\boldsymbol{A}_{\phi}^{\mathrm{T}}\boldsymbol{K}_{dM}\boldsymbol{X}_{\phi}\boldsymbol{\Sigma}_{M_{\phi}}^{-1}\boldsymbol{X}_{\phi}{}^{\mathrm{T}}\boldsymbol{K}_{Mr}}{k_{dd}-\boldsymbol{K}_{dU}\boldsymbol{A}_{\phi}\boldsymbol{\Sigma}_{\phi}^{-1}\boldsymbol{A}_{\phi}^{\mathrm{T}}\boldsymbol{K}_{Ud}} \tag{22}$$

Using Eq.(22), $\boldsymbol{D}_{\mathrm{KSSP}}$ can be calculated by kernel trick without any knowledge of the actual nonlinear mapping ϕ.

Through the above analysis, after choosing the kernel function and appropriate parameters, the KSSP algorithm is presented as follows.

Step 1 Construct the kernel matrix $\boldsymbol{K}_{UU}=\boldsymbol{U}_{\phi}^{\mathrm{T}}\boldsymbol{U}_{\phi}$, then calculate its rank N_b, matrix $\boldsymbol{\Sigma}_{\phi}$ which is composed by N_b nonzero eigenvalues and the related eigenvector matrix $\boldsymbol{A}_{\phi}$.

Step 2 Construct the kernel matrix $\boldsymbol{K}_{MM}=\boldsymbol{M}_{\phi}^{\mathrm{T}}\boldsymbol{M}_{\phi}$, then calculate its rank t, matrix $\boldsymbol{\Sigma}_{M\phi}$ which is composed by t nonzero eiegnvalues and the related eigenvector $\boldsymbol{X}_{\phi}$.

Step 3 Calculate $\boldsymbol{K}_{dM}$, $\boldsymbol{K}_{dU}$, $\boldsymbol{K}_{Ud}$, $\boldsymbol{K}_{UM}$ and k_{dd}, respectively

Step 4 For each pixel, calculate $\boldsymbol{K}_{Mr}$ and the projection $\boldsymbol{D}_{\mathrm{KSSP}}$ using Eq.(22).

4 ALGORITHM PERFERMANCE EVALUATED BY ROC ANALYSIS

A receiver operating characteristics (ROC) curves is a graph plotted by the detection power and versus the false alarm probability. The validity of the detector could be measured by the ROC analysis via the N-P detection theory. Instead of using common ROC analysis, Chang, *et al.* (1998) has defined measurement method called detection rate (*DR*), which calculates the area under an ROC curve for the effectiveness of the detector. Obviously, *DR* always lies between 1/2 and one. The worst case occurs when *DR* =1/2 , and the best case occurs when *DR* =1.

The estimation errors of the abundance obtained by SSP and KSSP reflect the penalties resulting from inaccurate estimation of unknown signature abundances. In order to evaluate the error performance of SSP and KSSP, we cast their associated estimation errors as a standard signal problem. In the following section, the performances of the two algorithms are evaluated by using ROC curve via N-P theory.

4.1 Neyman-Pearson theory

N-P theory is a signature detection method based on likelihood-ratio that maximum the detection probability for a fixed false alarm probability.

We assume that z is the projection resulting from a classifier q^{T} applied to the observed pixel r. A signal detection model based on z can be described by the test of two hypotheses as follows.

$$\begin{aligned} H_0 &: z=q^{\mathrm{T}}\boldsymbol{n}\cong p_o(z) \\ H_1 &: z=\alpha_p+q^{\mathrm{T}}\boldsymbol{n}\cong p_1(z) \end{aligned} \tag{23}$$

where the null hypothesis H_0 and the alternative hypothesis H_1 represent the case of noise existance alone and the case of the true target signature α_p presented in the z model, respectively.

The N-P detector associated with Eq.(23) is given by Eq.(24).

$$\delta_{NP}(z)=\begin{cases}1, & z=q^{\mathrm{T}}\boldsymbol{n}\geqslant\tau\\ 0, & z=q^{\mathrm{T}}\boldsymbol{n}<\tau\end{cases} \tag{24}$$

where τ is the threshold. Eq.(24)represents that H_0 is true when $z\geqslant\tau$ and H_1 is true when $z<\tau$.

From Eq.(24), we can also define the false alarm probability P_F and detection probability P_D as follows.

$$P_F=\int_{\tau}^{\infty}p_0(z)dz \tag{25}$$

$$P_D=\int_{\tau}^{\infty}p_1(z)dz \tag{26}$$

In Eq.(26), P_D specifies the capability of the detector in detecting the true target signature α_p. Therefore, the higher P_D, the smaller the estimation error becomes, the better performance of the detector shows.

4.2 The detection probability and false alarm probability of SSP

Substituting $\tilde{\boldsymbol{q}}_{\mathrm{SSP}}^{\mathrm{T}}$ specified by Eq.(5) for q^{T} in Eq.(23) results in a subpixel target detection model given by Eq.(7).

$$\begin{aligned} H_0 &: z=\tilde{\boldsymbol{q}}_{\mathrm{SSP}}^{\mathrm{T}}\boldsymbol{n}=\hat{n}_{\mathrm{SSP}}\cong p_o(z) \\ H_1 &: z=\alpha_p+\hat{n}_{\mathrm{SSP}}\cong p_1(z) \end{aligned} \tag{27}$$

where the noise $\hat{n}_{\mathrm{SSP}}$ is generated by the estimation error produced by SSP. The hypothesis H_0 represents the case in which the mixed pixel does not contain the target signature $\boldsymbol{d}$, while $\boldsymbol{H}_1$ indicated the presence of $\boldsymbol{d}$ in the mixed pixel.

Based on Eq.(7) and Eq.(27), we obtain the error covariance matrix $\boldsymbol{\Sigma}_{\mathrm{SSP}}$ as follows.

$$\boldsymbol{\Sigma}_{\mathrm{SSP}}=E\left[\varepsilon_{\mathrm{SSP}}\varepsilon_{\mathrm{SSP}}^{\mathrm{T}}\right]=E\left[\hat{n}_{\mathrm{SSP}}\hat{n}_{\mathrm{SSP}}^{\mathrm{T}}\right]=\sigma^2\frac{\boldsymbol{d}^{\mathrm{T}}\boldsymbol{P}_{\boldsymbol{U}}^{\perp}\boldsymbol{P}_{\boldsymbol{M}}\boldsymbol{P}_{\boldsymbol{M}}\boldsymbol{P}_{\boldsymbol{U}}^{\perp}\boldsymbol{d}}{\boldsymbol{d}^{\mathrm{T}}\boldsymbol{P}_{\boldsymbol{U}}^{\perp}\boldsymbol{d}\boldsymbol{d}^{\mathrm{T}}\boldsymbol{P}_{\boldsymbol{U}}^{\perp}\boldsymbol{d}}=\frac{\sigma^2}{\boldsymbol{d}^{\mathrm{T}}\boldsymbol{P}_{\boldsymbol{U}}^{\perp}\boldsymbol{d}} \tag{28}$$

We assume that $\boldsymbol{n}$ is a white Gaussian noise with zero mean and covariance matrix $\sigma^2\boldsymbol{I}$. Substituting Eq.(28) into Eq.(27) yields the equation.

$$p_o(z) \approx N(0, \sigma^2(\boldsymbol{d}^{\mathrm{T}}\boldsymbol{P}_{\boldsymbol{U}}^{\perp}\boldsymbol{d})^{-1})$$
$$p_1(z) \approx N(\alpha_p, \sigma^2(\boldsymbol{d}^{\mathrm{T}}\boldsymbol{P}_{\boldsymbol{U}}^{\perp}\boldsymbol{d})^{-1}) \tag{29}$$

and the threshold τ_{SSP} given by Eq.(30).

$$\tau_{\mathrm{SSP}} = \sigma(\boldsymbol{d}^{\mathrm{T}}\boldsymbol{P}_{\boldsymbol{U}}^{\perp}\boldsymbol{d})^{-1/2}\Phi^{-1}(1-P_F) \tag{30}$$

where $\Phi(x)$ is the cumulative distribution of the standard Gaussian random variable given by Eq.(31).

$$\Phi(x) = \int_{-\infty}^{x} \frac{1}{\sqrt{2\pi}} e^{-\frac{t^2}{2}} dt \tag{31}$$

And $\Phi^{-1}(x)$ is the inverse function of $\Phi(x)$.

The desired detection power P_{D_SSP} can be derived from Eq.(30)

$$P_{D\_\mathrm{SSP}} = 1-\Phi\left(\Phi^{-1}(1-P_F) - \frac{\alpha_p}{\sigma(\boldsymbol{d}^{\mathrm{T}}\boldsymbol{P}_{\boldsymbol{U}}^{\perp}\boldsymbol{d})^{-1/2}}\right) = 1-\Phi\left(\Phi^{-1}(1-P_F) - \sqrt{\mathrm{SNR}_{\mathrm{SSP,max}}}\right) \tag{32}$$

In Eq.(32), P_{D_SSP} is expressed in terms of $\boldsymbol{d}^{\mathrm{T}}\boldsymbol{P}_{\boldsymbol{U}}^{\perp}\boldsymbol{d}$, which measures the projection of $\boldsymbol{d}$ onto the orthogonal complement space $\langle \boldsymbol{U}^{\perp} \rangle$. The larger the projection is, the less similarity between $\boldsymbol{d}$ and $\boldsymbol{U}$ becomes, therefore, the better the discrimination. On the other hand, Eq.(32) illustrates that P_{D_SSP} is measured by the magnitude of SNR, the larger the SNR, the higher the detection power.

4.3 The detection probability and false alarm probability of KSSP

Substituing $\tilde{\boldsymbol{q}}_{\mathrm{SSP}\phi}^{\mathrm{T}}$ specified by Eq.(11) for q^{T} in Eq.(23) results in a subpixel target detection model given by the following equation.

$$H_0 : z = \tilde{\boldsymbol{q}}_{\mathrm{SSP}\phi}^{\mathrm{T}}\boldsymbol{n} = \hat{n}_{\mathrm{SSP}\phi} \cong p_o(z)$$
$$H_1 : z = \alpha_p + \hat{n}_{\mathrm{SSP}\phi} \cong p_1(z) \tag{33}$$

where the noise $\hat{n}_{\mathrm{SSP}\phi}$ is generated by the estimation error produced by SSP in feature space.

Based on Eq.(13) and Eq.(33), we obtain the error covariance matrix $\boldsymbol{\Sigma}_{\mathrm{SSP}\phi}$ as follows.

$$\boldsymbol{\Sigma}_{\mathrm{SSP}\phi} = E\left[\boldsymbol{\epsilon}_{\mathrm{SSP}\phi}\boldsymbol{\epsilon}_{\mathrm{SSP}\phi}^{\mathrm{T}}\right] = E\left[\hat{\boldsymbol{n}}_{\mathrm{SSP}\phi}\hat{\boldsymbol{n}}_{\mathrm{SSP}\phi}^{\mathrm{T}}\right] = \frac{\theta^2}{k_{\boldsymbol{dd}} - \boldsymbol{K}_{\boldsymbol{dU}}\boldsymbol{A}_{\phi}\boldsymbol{\Sigma}_{\phi}^{-1}\boldsymbol{A}_{\phi}^{\mathrm{T}}\boldsymbol{K}_{\boldsymbol{Ud}}} \tag{34}$$

Let us assume that $\boldsymbol{n}_{\phi}$ is a white Gaussian noise with zero mean and covariance matrix $\theta^2 I$. Substituting Eq.(34) into Eq.(33) yields.

$$p_o(z) \approx N(0, \theta^2(k_{\boldsymbol{dd}} - \boldsymbol{K}_{\boldsymbol{dU}}\boldsymbol{A}_{\phi}\boldsymbol{\Sigma}_{\phi}^{-1}\boldsymbol{A}_{\phi}^{\mathrm{T}}\boldsymbol{K}_{\boldsymbol{Ud}})^{-1})$$
$$p_1(z) \approx N(\alpha_p, \theta^2(k_{\boldsymbol{dd}} - \boldsymbol{K}_{\boldsymbol{dU}}\boldsymbol{A}_{\phi}\boldsymbol{\Sigma}_{\phi}^{-1}\boldsymbol{A}_{\phi}^{\mathrm{T}}\boldsymbol{K}_{\boldsymbol{Ud}})^{-1}) \tag{35}$$

and the threshold τ_{KSSP} given by Eq.(36).

$$\tau_{\mathrm{KSSP}} = \theta \frac{\Phi^{-1}(1-P_F)}{(k_{\boldsymbol{dd}} - \boldsymbol{K}_{\boldsymbol{dU}}\boldsymbol{A}_{\phi}\boldsymbol{\Sigma}_{\phi}^{-1}\boldsymbol{A}_{\phi}^{\mathrm{T}}\boldsymbol{K}_{\boldsymbol{Ud}})^{1/2}} \tag{36}$$

The desired detection power P_{D_KSSP} can be derived from Eq.(36).

$$P_{D\_\mathrm{KSSP}} = 1-\Phi\left(\Phi^{-1}(1-P_F) - \frac{\alpha_p}{\theta(k_{\boldsymbol{dd}} - \boldsymbol{K}_{\boldsymbol{dU}}\boldsymbol{A}_{\phi}\boldsymbol{\Sigma}_{\phi}^{-1}\boldsymbol{A}_{\phi}^{\mathrm{T}}\boldsymbol{K}_{\boldsymbol{Ud}})^{-1/2}}\right) = 1-\Phi\left(\Phi^{-1}(1-P_F) - \sqrt{\mathrm{SNR}_{\mathrm{SSP}\phi,\mathrm{max}}}\right) \tag{37}$$

In Eq.(37), P_{D_KSSP} is expressed in terms of $\phi(\boldsymbol{d})^{\mathrm{T}}\boldsymbol{P}_{\boldsymbol{U}\phi}^{\perp}\phi(\boldsymbol{d})$, the projection of $\boldsymbol{d}$ onto the orthogonal complement space $\langle \boldsymbol{U}^{\perp} \rangle$. The larger the projection is, the less similarity between $\boldsymbol{d}$ and $\boldsymbol{U}$ becomes, thus the better the discrimination. On the other hand, Eq.(37) illustrates that P_{D_KSSP} is measured by the magnitude of SNR, the larger the SNR is, the higher the detection power is.

5 EXPERIMENT RESULTS

The data sets used in the experimental are the mineral spectra from the U.S. Geological Survey (USGS) digital spectral library (Clark, 2007) and the Hyperspectral Digital Imagery Collection Experiment (HYDICE) urban image scene (Pazak, 2009).

5.1 Experiment using synthetic hyerspectral data

We select three spectral signatures from the USGS digital spectral library, which are Carnallite, Ammonioalunite, and Biotite. Fig. 2 shows these three endmember signatures with 224 spectral bands, Biotite is assumed as the object to be detected. The synthetic nonlinear mixture data is created by using the Hapke Model described by Wu, *et al.* (2006). In order to

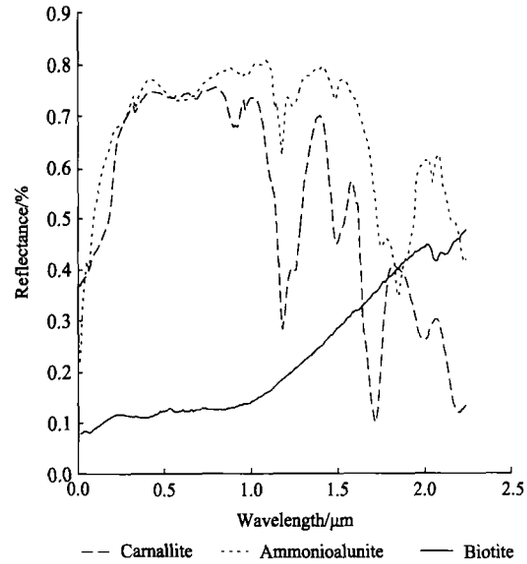

Fig. 2 Reflectances of carnallite, ammonioalunite, and biotite

demonstrate the effectiveness of KSSP for subpixel object detection, We use two different methods to create the abundance fractions, and Hapke model to generate two synthetic datasets. Each data set has 50 mixture pixels, and the angle of incidence is 30° and SNR is 30:1. There are two datasets as follows.

Datasets 1: Dirichlet distribution(Nascimento, *et al.*, 2005)

Abundance matrix $\boldsymbol{\alpha}$ of the mixed pixels is generated randomly according to a Dirichlet distribution.

Datasets 2: small probability object distribution

The abundance fractions of the 50 synthetic mixture pixels are shown in Table 1.

Table 1 Assigning relative abundances of endmembers for datasets 2

	1-19	20	21	...	29	30-50
Carnallite	0.5	0.45	0.455	...	0.495	0.5
Ammonioalunite	0.5	0.45	0.455	...	0.495	0.5
Biotite	0	0.1	0.09	...	0.01	0

Since the real abundance of the synthetic mixture pixels is known prior, to evaluate the performance of the SSP and KSSP algorithms, the correlation coefficients (Tao, *et al*, 2008), the abundance angle distance (AAD) (Miao, *et al.*, 2007) and the root mean square error (RMSE) are used to measure the similarity between the true abundances and the estimated abundances. Furthermore, the ROC curve described in section 4 is used to evaluate the detection performance of the two algorithms.

By several experiments, the kernel parameters of KSSP was chosen as a=0.001, b=0.2, c= −0.01 for datasets 1 and a=0.1, b=0.01, c=0.8 for datasets 2. Table 2 and Table 3 give the three performance comparisons of the SSP and KSSP for datasets 1 and datasets 2. The detection result curve of datasets 1 and datasets 2 are shown in Fig.3(a) and Fig.3(b). Fig.4 is the ROC curves produced by SSP and KSSP with SNR = 30.

Fig.3 shows that the result obtained by KSSP is very similarly with real abundance, and it also shows that the KSSP obviously restrains the noise. The performance comparison in Table 2 and Table 3 demonstrate that all the three performances of KSSP are better than SSP. Furthermore, Fig.4 shows that KSSP outperforms the conventional SSP approach.

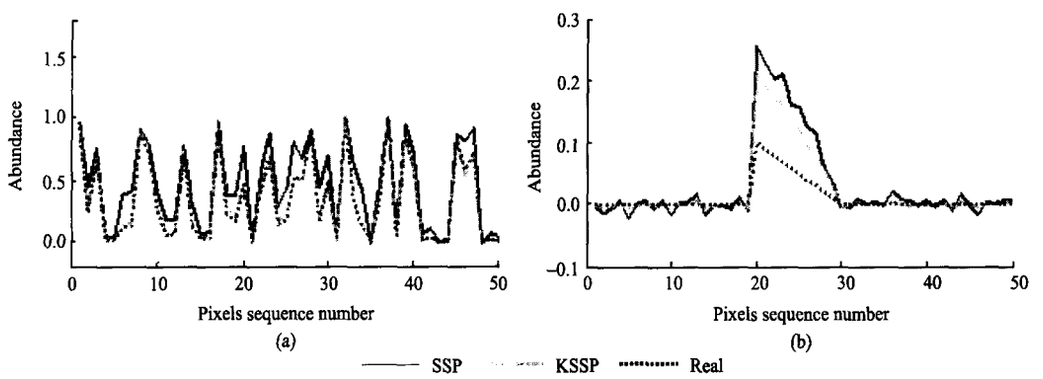

Fig. 3 Comparison between performance curves generated by SSP, KSSP and real abundance

(a) datasets 1; (b) datasets 2

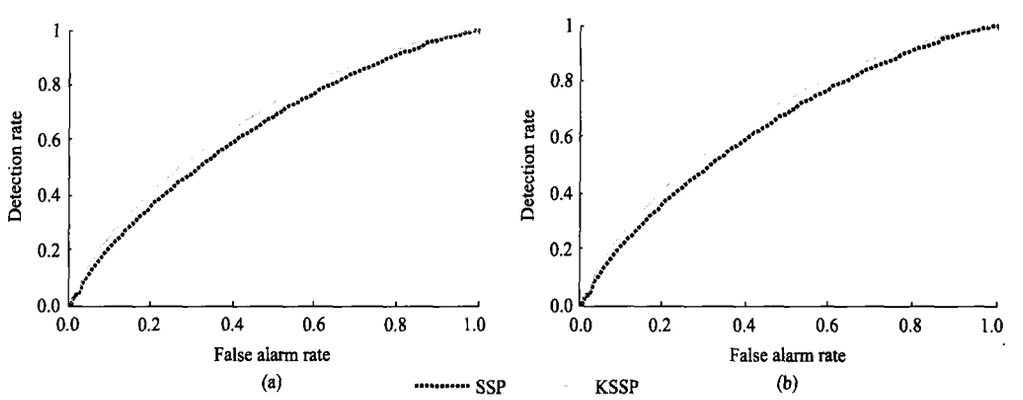

Fig. 4 ROC curves produced by SSP and KSSP

(a) datasets 1; (b) datasets 2

Table 2 The performance comparison between target abundances from SSP & KSSP and the real abundance based on Cor, AAD and RMSE for datasets 1

	Cor	AAD	RMSE
SSP	0.957691	0.231915	0.153329
KSSP	0.998236	0.0459696	0.0223425

Table 3 The performance comparison between target abundances from SSP & KSSP and the real abundance based on Cor, AAD and RMSE for datasets 2

	Cor	AAD	RMSE
SSP	0.986418	0.151409	0.0487654
KSSP	0.996017	0.081963	0.0338377

5.2 Experiment for real image

For the experiments on real data, we selected a 307×307 pixel urban image scene (Fig. 5) from AVIRIS data extracted from the Hyperspectral Digital Imagery Collection Experiment (HYDICE). It is composed of 210 spectral channels. To improve the unmixing performance, we have removed bands with low SNR and the water-vapor absorption bands (including bands 1—4, 76, 87, 101—111, 136—153, and 198—210) from the original 210 band data cube. Therefore, a total of 162 bands are used in the experiment.

Fig. 5 Urban hyperspectral data set (band 50)

This region contains a mixture of man-made objects and forestry. There are four targets of interest: asphalt, roof, grass and tree. Owing to the spectral variability, the reference endmember spectra are manually chosen from the hyperspectral data (e.g., the spectrum in the coordinate position of [197, 62] is selected as the asphalt spectrum).

In this experiment, we choose the RBF kernel as the kernel function of KSSP. Its parameter $2\sigma^2$ is proved by experiments to be between Eq.(2) and Eq.(5). Fig.6 is the detect result of SSP for the object asphalt, roofs, grass and trees respectively. Fig.7 is the results of KSSP for the four objects with $2\sigma^2=4$, where figures labeled by Fig.7(a), Fig.7(b), Fig.7(c) and Fig.7(d) are results for asphalt, roofs, grass and trees respectively. In Fig. 6 and Fig.7, pure black denotes that the abundance of a certain material in this pixel is 0%, whereas pure white denotes 100%. As shown in these figures, each object is detected, but the results of SSP are more blurry than that of KSSP.

(a) (b) (c) (d)

Fig. 6 Detection results for the four targets in urban hyperspectral data set using SSP
(a) Asphalt; (b) Roofs; (c) Grass; (d) Trees

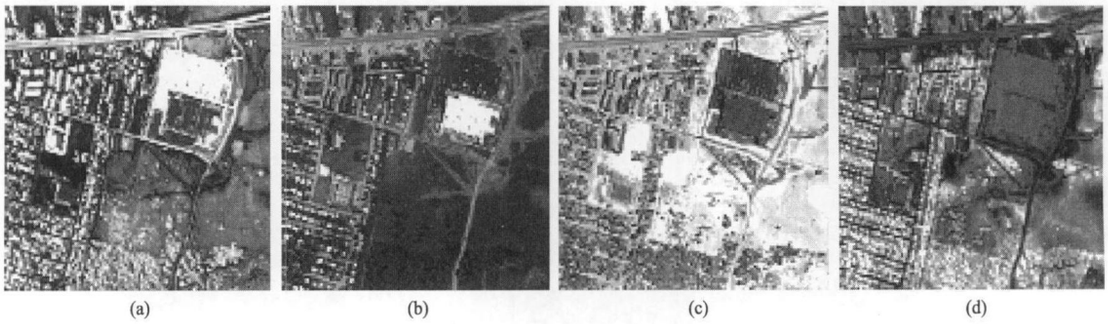

(a) (b) (c) (d)

Fig. 7 Detection results for the four targets in urban hyperspectral data set using KSSP
(a) Asphalt; (b) Roofs; (c) Grass; (d) Trees

6 CONCLUTION

In this paper, a kernel-based signature space orthogonal projection (KSSP) technique is proposed for nonlinear subpixel target detection in hyperspectral imagery. By mean of kernel trick, mixed pixels are implicitly mapped nonlinearly into a high-dimensional feature space to satisfy linear mixed in the feature space and to detect the objects using SSP in the feature space. The KSSP using the kernel function could keep the better performance of nonlinear method as well as avoid

complex computation of the nonlinear mapping. Experimental results demonstrate that the proposed KSSP approach outperforms the SSP method in target detection, and improves robustness to noise.

REFERENCES

Bian Z Q and Zhang X G. 2000. Pattern Recognition. Beijing: Tsinghua University Press: 224–226

Chang C I, Zhao X L, Althouse M L G and Pan J J. 1998. Least squares subspace projection approach to mixed pixel classification for hyperspectral images. *IEEE Transactions on Geoscience and Remote Sensing*, **36**(3): 898–912

Capobianco L and Camps-Valls G. 2008. Target detection with a contextual kernel orthogonal subspace projection. Image and Signal Processing for Remote Sensing XIV, SPIE Digital Library, Cardiff, UK

Clark R N. 2007. Spectral Library 06. USGS Digital Spectral Libraries[DB/OL]. [2009-05-10]. http://speclab.cr.usgs.gov

Jia S. 2007. Unsupervised hyperspectral unmxiing Theory and Techniques. Hangzhou: Zhejiang University: 69

Kwon H and Nasrabadi N M. 2005. Kernel orthogonal subspace projection for hyperspectral signal classification. *IEEE Transactions on Geoscience and Remote Sensing*, **43**(12): 2952–2962

Miao L D and Qi H R. 2007. Endmember extraction from highly mixed data using minimum volume constrained nonnegative matrix factorization. *IEEE Transactions on Geoscience and Remote Sensing*, **45**(3): 765–777

Nascimento J M P and Dias J M B. 2005. Vertex component analysis: a fast algorithm to unmix hyperspectral data. *IEEE Transactions on Geoscience and Remote Sensing*, **43**(4): 898– 910

Pazak R. 2009. Hypercube. URBAIN.zip [EB/OL]. [2009-08-02]. http:// www. tec.army.mil/ Hypercube

Shawe-Taylor J and Cristianini N. 2005. Kernel methods for pattern analysis. Beijing: China machine press: 20–42

Tong Q X, Zhang B and Zheng L F. 2006. Hyperspectral Remote Sensing. Beijing: Higher Education Press: 255–262

Tao X T, Wang B and Zhang L M. 2008. New scheme for decomposition of mixed pixels of remote sensing images based on nonnegative matrix factorization. *Information and Electronic Engineering*, **6**(1): 34–39

Wu B, Zhang L P and Li P X. 2006. Unmixing hyperspectral imagery based on support vector nonlinear approximating regression. *Journal of Remote Sensing*, **10**(3): 312–318

高光谱图像目标检测的核信号空间正交投影法

赵辽英[1], 张凯[1], 厉小润[2]

1. 杭州电子科技大学 计算机应用技术研究所, 浙江 杭州 310018;
2. 浙江大学 电气工程学院, 浙江 杭州 310027

摘 要: 针对非线性混合下的亚像元目标检测问题, 提出一种基于核函数的信号空间正交投影方法(KSSP)。该方法作为信号空间正交投影方法(SSP)的非线性推广, 首先将原空间中像元矢量经非线性映射转换到高维特征空间, 然后在特征空间中用线性信号空间正交投影进行目标检测。通过核技巧, 核信号空间正交投影不必知道具体的非线性映射形式。经模拟数据与真实高光谱图像数据实验证明, KSSP 方法在目标检测性能上优于 SSP, 且对噪声的抑制也有很好的效果。

关键词: 信号空间正交投影, 核函数, 亚像元目标检测, 核信号空间正交投影

中图分类号: TP391 **文献标志码:** A

引用格式: 赵辽英, 张凯, 厉小润. 2011. 高光谱图像目标检测的核信号空间正交投影法. 遥感学报, **15**(1): 13–28
Zhao L Y, Zhang K and Li X R. 2011. Kernel signature space orthogonal projection for target detection in hyperspectral imagery. *Journal of Remote Sensing*, **15**(1): 13–28

1 引 言

利用高光谱图像进行目标检测和识别是遥感图像处理领域的研究热点之一。由于遥感图像的空间分辨率的限制以及地物的复杂多样性, 使得某些感兴趣目标在图像中只能以亚像元的形式存在, 即图像中只存在感兴趣目标与别的地物的混合像元。亚像元目标检测和识别是提高高光谱遥感应用的关键技术之一。

通常实际应用中, 在已经知道或通过某种方法得到目标和背景端元光谱信息的前提下, 近似计算目标和背景端元的光谱分布(丰度值), 判断高光谱图像中的目标点是否存在。目前常用的方法包括最小二乘法、正交子空间投影算法(OSP)、信号空间正交投影算法(SSP)等(Chang, 1998), 这些方法都是基于线性混合模型提出的。

光谱混合从本质上可以分为线性混合和非线性混合两种模式。线性光谱混合模型具有构模简单, 物理含义明确的优点, 理论上也有较好的科学性, 但线性混合模型适用于本质上就属于或者基本属于线性混合的地物, 以及在大尺度上可以认为是线性混合的地物。对于一些微观尺度上地物的精细光谱分析或一些小概率目标的检测来说, 就需要用非线性混合模型来解释。目前比较典型且有一定影响力的光谱混合模型有 Hapke 模型, Kubelk-Munk 模型, 基于辐射通量密度理论的植被、土壤光谱混合模型, SAIL 模型等(童庆禧等, 2006)。然而, 这些非线性混合模型都有各自的适用范围, 局限性大, 并且非线性混合模型的探索也十分困难。

随着支持向量机(SVM)在各领域中的成功应用, 通过核函数方法, 使得线性方法能够处理非线性问题已成为机器学习的一热点方向。核函数方法是一种可以避免确定非线性关系和计算非线性模型的有效的非线性数据分析方法(Shawe-Tylor, 2005)。近年来, 核函数方法在高光谱遥感图像的分类和目标检测中得到较多的应用, 特别是美国军事研究实验室的 Kwon 等(2005)对子空间匹配检测器 (MSD)、光谱匹配滤波器(SMF)、 自适应子空间检测器(ASD), 正交子空间投影方法进行了非线性推广, 提出了核子空间匹配检测器 (KMSD)、核光谱匹配滤波器(KSMF)、核自适应子空间检测器(KASD)和核正交子空间投影(KOSP)算法。另外, Capobianco 等(2008)

收稿日期: 2009-12-21; **修订日期:** 2010-04-22
基金项目: 浙江省自然科学基金资助, 资助项目编号为: Y1100196。
第一作者简介: 赵辽英(1970—), 女, 副教授, 博士, 主要研究方向为模式识别、遥感图像分析。E-mail: zhaoly@hdu.edu.cn.

对 KOSP 做了进一步的研究，提出了基于上下文的 KOSP。

SSP 是 Chang 等(1998)依据最小平方误差原理，在 KOSP 的基础上提出的一种后验正交子空间投影方法。本文借鉴 KOSP 算法思想，运用核函数理论，将 SSP 推广到非线性空间中，提出了核信号空间正交投影(KSSP)算法。KSSP 通过非线性映射将高光谱数据映射到高维特征空间，使光谱数据在特征空间中满足线性混合模型，再用线性 SSP 实现目标检测。为了评价 SSP 与 KSSP 的有效性，本文把其估计的误差作为 N-P(Neyman-Pearson)理论中的信号检测问题，再通过 ROC (Receiver Operating Characteristic Curve) 曲线来评价两种算法性能。仿真数据实验和实际遥感数据实验结果均表明 KSSP 有效地解决了非线性高光谱混合数据的目标检测问题，且大大抑制了噪声，性能优于 SSP。

2 信号空间正交投影

设 $\boldsymbol{r}$ 为 $L\times1$ 维的观测光谱向量，$\boldsymbol{M}$ 为 $L\times p$ 维端元矩阵(p 为端元数)，α为 $p\times1$ 维的端元丰度向量，n 为 $L\times1$ 维的附加噪声向量，则线性光谱混合模型(LSMM)可表示为

$$\boldsymbol{r}=\boldsymbol{M}\boldsymbol{\alpha}+\boldsymbol{n} \tag{1}$$

OSP 和 SSP 认为所有像元均由感兴趣目标信号 $\boldsymbol{d}$ 和背景端元 $\boldsymbol{U}$ 两部分组成。不失一般性，设 $\boldsymbol{d}=\boldsymbol{m}_i$,$1\leqslant i\leqslant p$，则背景端元矢量空间 $\boldsymbol{U}=(\boldsymbol{m}_1,\cdots,\boldsymbol{m}_{i-1},\boldsymbol{m}_{i+1},\cdots,\boldsymbol{m}_p)$。因此，式(1)可以写为

$$\boldsymbol{r}=\boldsymbol{d}\alpha_i+\boldsymbol{U}\gamma+\boldsymbol{n} \tag{2}$$

式中，α_i 为 $\boldsymbol{m}_i$ 的丰度值，$\gamma=(\alpha_1,\cdots,\alpha_{i-1},\alpha_{i+1},\cdots,\alpha_p)^{\mathrm{T}}$ 为对应背景端元的丰度值。

OSP 是在丰度已知的情况下根据信噪比最小推导出的，然而实际中丰度往往是不知道的，需要从数据本身来估计丰度。引入后验模型:

$$\boldsymbol{r}=\boldsymbol{M}\hat{\boldsymbol{\alpha}}+\hat{\boldsymbol{n}}=\boldsymbol{d}\hat{\alpha}_i+\boldsymbol{U}\hat{\gamma}+\hat{\boldsymbol{n}} \tag{3}$$

式中 $\hat{\boldsymbol{\alpha}},\hat{\alpha}_i$ 和 $\hat{\gamma}$ 分别为$\boldsymbol{\alpha},\alpha_i$ 和γ的估计。

SSP 首先将像元矢量 $\boldsymbol{r}$ 投影到 $\boldsymbol{M}=\langle\boldsymbol{U},\boldsymbol{d}\rangle$ 上，然后再投影到背景信号子空间的正交补空间 $\langle\boldsymbol{U}^{\perp}\rangle$ 上，最后投影到目标信号 $\langle\boldsymbol{d}\rangle$ 上，形成一个分类器(图 1)。其中 $\boldsymbol{P}_{\boldsymbol{M}}=\boldsymbol{M}(\boldsymbol{M}^{\mathrm{T}}\boldsymbol{M})^{-1}\boldsymbol{M}^{\mathrm{T}}$ 为信号空间正交投影，$\boldsymbol{P}_{\boldsymbol{U}}^{\perp}=\boldsymbol{I}-\boldsymbol{U}(\boldsymbol{U}^{\mathrm{T}}\boldsymbol{U})^{-1}\boldsymbol{U}^{\mathrm{T}}$ 为背景信号子空间的正交补投影，

$$\boldsymbol{q}_{\mathrm{SSP}}^{\mathrm{T}}=\boldsymbol{d}^{\mathrm{T}}\boldsymbol{p}_{\boldsymbol{U}}^{\perp}\boldsymbol{P}_{\boldsymbol{M}} \tag{4}$$

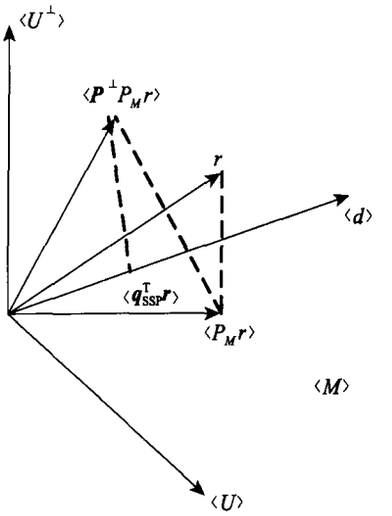

图 1 信号空间正交投影

为最终分类器。

由于 $\boldsymbol{d}^{\mathrm{T}}\boldsymbol{P}_{\boldsymbol{U}}^{\perp}\boldsymbol{d}=\boldsymbol{d}^{\mathrm{T}}\boldsymbol{P}_{\boldsymbol{U}}^{\perp}\boldsymbol{P}_{\boldsymbol{M}}\boldsymbol{d}$，归一化的 SSP 分类器为:

$$\tilde{\boldsymbol{q}}_{\mathrm{SSP}}^{\mathrm{T}}=\frac{\boldsymbol{q}_{\mathrm{SSP}}^{\mathrm{T}}}{\boldsymbol{d}^{\mathrm{T}}\boldsymbol{P}_{\boldsymbol{U}}^{\perp}\boldsymbol{d}} \tag{5}$$

像元矢量 $\boldsymbol{r}$ 经过归一化 SSP 投影的结果:

$$D_{\mathrm{SSP}}(\boldsymbol{r})=\frac{\boldsymbol{q}_{\mathrm{SSP}}^{\mathrm{T}}\boldsymbol{r}}{\boldsymbol{d}^{\mathrm{T}}\boldsymbol{P}_{\boldsymbol{U}}^{\perp}\boldsymbol{d}}=\frac{\boldsymbol{d}^{\mathrm{T}}\boldsymbol{P}_{\boldsymbol{U}}^{\perp}\boldsymbol{P}_{\boldsymbol{M}}\boldsymbol{r}}{\boldsymbol{d}^{\mathrm{T}}\boldsymbol{P}_{\boldsymbol{U}}^{\perp}\boldsymbol{d}} \tag{6}$$

将式(2)、(3)、(4)联立，使用最小平方误差作为最优化准则可得丰度估计误差和最大输出信噪比为(Chang, 1998)

$$\varepsilon=D_{\mathrm{SSP}}-\alpha_i=\frac{\boldsymbol{d}^{\mathrm{T}}\boldsymbol{P}_{\boldsymbol{U}}^{\perp}\boldsymbol{P}_{\boldsymbol{M}}\boldsymbol{n}}{\boldsymbol{d}^{\mathrm{T}}\boldsymbol{P}_{\boldsymbol{U}}^{\perp}\boldsymbol{d}} \tag{7}$$

$$\mathrm{SNR}_{\mathrm{SSP,max}}=\frac{\alpha_i^2}{\sigma^2}\boldsymbol{d}^{\mathrm{T}}\boldsymbol{P}_{\boldsymbol{U}}^{\perp}\boldsymbol{d} \tag{8}$$

式中，σ为噪声根方差。$\boldsymbol{d}^{\mathrm{T}}\boldsymbol{P}_{\boldsymbol{U}}^{\perp}\boldsymbol{d}$ 为归一化因子。当 $\boldsymbol{d}$ 和 $\boldsymbol{U}$ 相关性较大时，该值将较小，信噪比变小。因此，归一化因子可以用来衡量投影算子对目标的检测能力。

3 核信号空间正交投影

3.1 特征空间中的 LSMM 与 SSP

线性混合是非线性混合在多次反射被忽略的情况下的特例，如果通过非线性映射 ϕ将所有像元光谱数据映射到一个高维的特征空间 $\boldsymbol{H}$ 中，并使所有像元在特征空间中的多次反射最小，则特征空间中的混合像元可以近似为线性混合。设 $\boldsymbol{M}_{\phi}$是特征空间中的端元光谱矩阵，α是各端元对应的像元组份，$\boldsymbol{n}_{\phi}$

为特征空间中的随机噪声, 则特征空间中线性混合模型可表示为:

$$\phi(\boldsymbol{r})=\boldsymbol{M}_\phi\boldsymbol{\alpha}+\boldsymbol{n}_\phi \tag{9}$$

对应于式(2), 模型(9)可进一步表示为:

$$\phi(\boldsymbol{r})=\phi(\boldsymbol{d})\alpha_i+\boldsymbol{U}_\phi\boldsymbol{\gamma}+\boldsymbol{n}_\phi \tag{10}$$

式中, $\phi(\boldsymbol{d})$为特征空间中感兴趣目标信号, α_i为其相应的组份; $\boldsymbol{U}_\phi$为特征空间 $\boldsymbol{H}$ 中非感兴趣背景信号, $\boldsymbol{\gamma}$ 为其相应的组份。

根据式(5)的 SSP 算子及以上特征空间中的 LSMM 的推导, 很容易得出特征空间中像元矢量 $\boldsymbol{r}$ 经过归一化 SSP 投影的结果:

$$\tilde{\boldsymbol{q}}_{\mathrm{SSP}\phi}^{\mathrm{T}}=\frac{\phi(\boldsymbol{d})^{\mathrm{T}}\boldsymbol{P}_{U_\phi}^{\perp}\boldsymbol{P}_{M_\phi}}{\phi(\boldsymbol{d})^{\mathrm{T}}\boldsymbol{P}_{U_\phi}^{\perp}\phi(\boldsymbol{d})} \tag{11}$$

$$D_{\mathrm{SSP}\phi}(\boldsymbol{r})=\frac{\phi(\boldsymbol{d})\boldsymbol{P}_{U_\phi}^{\perp}\boldsymbol{P}_{M_\phi}\phi(\boldsymbol{r})}{\phi(\boldsymbol{d})^{\mathrm{T}}\boldsymbol{P}_{U_\phi}^{\perp}\phi(\boldsymbol{d})} \tag{12}$$

式中, $\boldsymbol{P}_{M_\phi}=\boldsymbol{M}_\phi(\boldsymbol{M}_\phi^{\mathrm{T}}\boldsymbol{M}_\phi)^{-1}\boldsymbol{M}_\phi^{\mathrm{T}}$, $\boldsymbol{P}_{U_\phi}^{\perp}=\boldsymbol{I}_\phi-\boldsymbol{U}_\phi\boldsymbol{U}_\phi^{\#}=\boldsymbol{I}_\phi-\boldsymbol{U}_\phi(\boldsymbol{U}_\phi{}^{\mathrm{T}}\boldsymbol{U}_\phi)^{-1}\boldsymbol{U}_\phi{}^{\mathrm{T}}$, $\boldsymbol{I}_\phi$是特征空间中的单位矩阵。

相应的丰度估计误差和最大输出信噪比为:

$$\varepsilon=\frac{\phi(\boldsymbol{d})\boldsymbol{P}_{U_\phi}^{\perp}\boldsymbol{P}_{M_\phi}\boldsymbol{n}_\phi}{\phi(\boldsymbol{d})^{\mathrm{T}}\boldsymbol{P}_{U_\phi}^{\perp}\phi(\boldsymbol{d})} \tag{13}$$

$$\mathrm{SNR}_{\mathrm{SSP}\phi,\max}=\frac{\alpha_i^2}{\theta^2}\phi(\boldsymbol{d})^{\mathrm{T}}\boldsymbol{P}_{U_\phi}^{\perp}\phi(\boldsymbol{d}) \tag{14}$$

式中, θ为特征空间中的噪声根方差。

由于 ϕ 的具体表达式通常很难确定, 式(11)—式(14)不能直接应用。然而, 通过核技巧, 可以把式(11)—式(14)转化为核函数的形式, 而不需要知道 ϕ 的具体表达式。

3.2 KSSP 算法

这部分主要介绍如何运用核技巧将特征空间中的 SSP 核化, 相应的算法称为核信号空间正交投影(KSSP)。先给出核函数定义。

定义 1(核函数) 对所有 $\boldsymbol{x},\boldsymbol{z}\in\boldsymbol{X}$, $\boldsymbol{X}\subset\mathbf{R}^n$, 若函数 k 满足

$$k(\boldsymbol{x},\boldsymbol{z})=\langle\phi(\boldsymbol{x})\cdot\phi(\boldsymbol{z})\rangle \tag{15}$$

则称 k 为核函数。其中ϕ是从输入空间 $\boldsymbol{X}$ 到内积特征空间 $\boldsymbol{H}$ 的映射, $\langle\cdot\rangle$ 表示内积。

任何满足 Mercer 定理或正定性的函数都可以作为核函数(Shawe-Taylor, 2005), 常用的简单核函数有 RBF 核函数: $k(\boldsymbol{x},\boldsymbol{z})=\exp\left(-\frac{\|\boldsymbol{x}-\boldsymbol{z}\|^2}{2\sigma^2}\right)$, 其中$\sigma$为核参数; 多项式核函数: $k(\boldsymbol{x},\boldsymbol{z})=(a\boldsymbol{x}^{\mathrm{T}}\boldsymbol{z}+c)^b$, 其中 a、b、c 为核参数。

根据核函数的定义, 矩阵 $\boldsymbol{K}_{UU}=\boldsymbol{U}_\phi^{\mathrm{T}}\boldsymbol{U}_\phi$ 和 $\boldsymbol{K}_{MM}=\boldsymbol{M}_\phi^{\mathrm{T}}\boldsymbol{M}_\phi$ 的每个元素为一个核函数, $\boldsymbol{K}_{UU}$ 和 $\boldsymbol{K}_{MM}$称为核函数矩阵。

为了将式(12)表示成关于核函数的表达式, 先对 $\boldsymbol{K}_{UU}$和 $\boldsymbol{K}_{MM}$做进一步的分析。

设 $\boldsymbol{U}_\phi^{\mathrm{T}}\boldsymbol{U}_\phi$ 的秩为 N_b, $\lambda_i(i=1,2,\cdots,N_b)$ 为矩阵 $\boldsymbol{U}_\phi^{\mathrm{T}}\boldsymbol{U}_\phi$ 的非零特征值, $\boldsymbol{\Sigma}_\phi=\mathrm{diag}(\lambda_1,\lambda_2,\cdots,\lambda_{N_b})$, $\boldsymbol{A}_\phi=[\boldsymbol{a}_\phi^1,\boldsymbol{a}_\phi^2,\cdots,\boldsymbol{a}_\phi^{N_b}]$ 是 $\boldsymbol{U}_\phi^{\mathrm{T}}\boldsymbol{U}_\phi$ 与 $\boldsymbol{\Sigma}_\phi$ 对应的特征向量矩阵, 则根据奇异值分解定理及推论(边肇棋等, 2000)得

$$\boldsymbol{U}_\phi^{\mathrm{T}}\boldsymbol{U}_\phi=\boldsymbol{A}_\phi\boldsymbol{\Sigma}_\phi\boldsymbol{A}_\phi^{\mathrm{T}} \tag{16}$$

因此,

$$\boldsymbol{P}_{U_\phi}=\boldsymbol{U}_\phi\boldsymbol{A}_\phi\boldsymbol{\Sigma}_\phi^{-1}\boldsymbol{A}_\phi^{\mathrm{T}}\boldsymbol{U}_\phi^{\mathrm{T}} \tag{17}$$

$$\boldsymbol{P}_{U_\phi}^{\perp}=\boldsymbol{I}_\phi-\boldsymbol{U}_\phi\boldsymbol{A}_\phi\boldsymbol{\Sigma}_\phi^{-1}\boldsymbol{A}_\phi^{\mathrm{T}}\boldsymbol{U}_\phi^{\mathrm{T}} \tag{18}$$

同理, 设 $\boldsymbol{M}_\phi^{\mathrm{T}}\boldsymbol{M}_\phi$ 的秩为 t, υ_i 为矩阵 $\boldsymbol{M}_\phi^{\mathrm{T}}\boldsymbol{M}_\phi$ 的非零特征值, $\boldsymbol{\Sigma}_{M\phi}=\mathrm{diag}(\upsilon_1,\upsilon_2,\cdots,\upsilon_t)$, $\boldsymbol{X}_\phi$为 $\boldsymbol{M}_\phi^{\mathrm{T}}\boldsymbol{M}_\phi$ 与 $\boldsymbol{\Sigma}_{M\phi}$对应的特征向量矩阵, 则

$$\boldsymbol{M}_\phi^{\mathrm{T}}\boldsymbol{M}_\phi=\boldsymbol{X}_\phi\boldsymbol{\Sigma}_{M\phi}\boldsymbol{X}_\phi^{\mathrm{T}} \tag{19}$$

因此,

$$\boldsymbol{P}_{M_\phi}=\boldsymbol{M}_\phi\boldsymbol{X}_\phi\boldsymbol{\Sigma}_{M\phi}^{-1}\boldsymbol{X}_\phi{}^{\mathrm{T}}\boldsymbol{M}_\phi{}^{\mathrm{T}} \tag{20}$$

将式(18)、式(20)代入式(12), 得:

$$D_{\mathrm{SSP}\phi}(\boldsymbol{r})=\frac{\phi(\boldsymbol{d})^{\mathrm{T}}\boldsymbol{M}_\phi\boldsymbol{X}_\phi\boldsymbol{\Sigma}_{M_\phi}^{-1}\boldsymbol{X}_\phi{}^{\mathrm{T}}\boldsymbol{M}_\phi{}^{\mathrm{T}}\phi(\boldsymbol{r})-\phi(\boldsymbol{d})^{\mathrm{T}}\boldsymbol{U}_\phi\boldsymbol{A}_\phi\boldsymbol{\Sigma}_\phi^{-1}\boldsymbol{A}_\phi^{\mathrm{T}}\boldsymbol{U}_\phi^{\mathrm{T}}\boldsymbol{M}_\phi\boldsymbol{X}_\phi\boldsymbol{\Sigma}_{M_\phi}^{-1}\boldsymbol{X}_\phi{}^{\mathrm{T}}\boldsymbol{M}_\phi{}^{\mathrm{T}}\phi(\boldsymbol{r})}{\phi(\boldsymbol{d})^{\mathrm{T}}\phi(\boldsymbol{d})-\phi(\boldsymbol{d})^{\mathrm{T}}\boldsymbol{U}_\phi\boldsymbol{A}_\phi\boldsymbol{\Sigma}_\phi^{-1}\boldsymbol{A}_\phi^{\mathrm{T}}\boldsymbol{U}_\phi^{\mathrm{T}}\phi(\boldsymbol{d})} \tag{21}$$

同样, 向量 $\phi(\boldsymbol{d})^{\mathrm{T}}\boldsymbol{M}_\phi$, $\boldsymbol{M}_\phi{}^{\mathrm{T}}\phi(\boldsymbol{r})$, $\phi(\boldsymbol{d})^{\mathrm{T}}\boldsymbol{U}_\phi$, $\boldsymbol{U}_\phi^{\mathrm{T}}\phi(\boldsymbol{d})$ 的每个元素都是一个核函数值, 将这些向量分别记为 $\boldsymbol{K}_{dM}$, $\boldsymbol{K}_{Mr}$, $\boldsymbol{K}_{dU}$和 $\boldsymbol{K}_{Ud}$, 矩阵 $\boldsymbol{U}_\phi^{\mathrm{T}}\boldsymbol{M}_\phi$ 中每个元素也是一个核函数值, 记为 $\boldsymbol{K}_{UM}$, $k_{dd}=\phi(\boldsymbol{d})^{\mathrm{T}}\phi(\boldsymbol{d})$ 为一个核函数值。于是, 式(21)可简写为:

$$D_{\mathrm{KSSP}}(\boldsymbol{r})=\frac{\boldsymbol{K}_{dM}\boldsymbol{X}_\phi\boldsymbol{\Sigma}_{\mathrm{M}_\phi}^{-1}\boldsymbol{X}_\phi{}^{\mathrm{T}}\boldsymbol{K}_{Mr}-\boldsymbol{K}_{dU}\boldsymbol{A}_\phi\boldsymbol{\Sigma}_\phi^{-1}\boldsymbol{A}_\phi^{\mathrm{T}}\boldsymbol{K}_{dM}\boldsymbol{X}_\phi\boldsymbol{\Sigma}_{\mathrm{M}_\phi}^{-1}\boldsymbol{X}_\phi{}^{\mathrm{T}}\boldsymbol{K}_{Mr}}{k_{dd}-\boldsymbol{K}_{dU}\boldsymbol{A}_\phi\boldsymbol{\Sigma}_\phi^{-1}\boldsymbol{A}_\phi^{\mathrm{T}}\boldsymbol{K}_{Ud}} \tag{22}$$

通过运用核技巧, 不需要知道具体的非线性映射函数 ϕ 就可以求出 D_{KSSP}。

通过上述分析，选定核函数及参数后，KSSP 算法过程描述如下：

步骤 1 计算核函数矩阵 $\boldsymbol{K}_{UU}=\boldsymbol{U}_{\phi}^{\mathrm{T}}\boldsymbol{U}_{\phi}$，求出秩 N_b，求 $\boldsymbol{K}_{UU}$ 的 N_b 个非零特征值和相应特征向量，得到 $\boldsymbol{\Sigma}_{\phi}$ 和 $\boldsymbol{A}_{\phi}$。

步骤 2 计算核函数矩阵 $\boldsymbol{K}_{MM}=\boldsymbol{M}_{\phi}^{\mathrm{T}}\boldsymbol{M}_{\phi}$，求出秩 t，求 $\boldsymbol{K}_{MM}$ 的 t 个非零特征值和相应特征向量，得到 $\boldsymbol{\Sigma}_{M\phi}$ 和 $\boldsymbol{X}_{\phi}$。

步骤 3 分别计算 $\boldsymbol{K}_{dM}$, $\boldsymbol{K}_{dU}$、$\boldsymbol{K}_{Ud}$、$\boldsymbol{K}_{UM}$ 和 k_{dd}。

步骤 4 对每个像元计算 $\boldsymbol{K}_{Mr}$，根据式(22)求得投影结果 $\boldsymbol{D}_{\mathrm{KSSP}}$。

4 ROC 曲线评价算法性能

ROC 曲线是反映检测概率随虚警概率变化而变化的曲线。ROC 曲线根据 N-P 理论可作为检测器准确性评价的性能指标。不同于一般的 ROC 曲线分析，Chang 等(1998)通过计算 ROC 曲线下面积–检测率 DR 作为性能指标来评估算法性能。$1/2\leqslant DR\leqslant 1$，显然，当 $DR=1/2$ 时结果最差，当 $DR=1$ 时结果最好。

SSP 和 KSSP 的丰度估计误差反映了算法对真实丰度的非精确估计的惩罚结果。SSP 和 KSSP 算法可作为检测器用来检测混合像元中是否存在目标信号，而两种检测器的有效性取决于估计丰度的准确性。下面通过 N-P 准则用 ROC 曲线作为两种检测算法的性能指标。

4.1 N-P 准则

N-P 准则是在给定虚警概率的前提下，使检测概率最大的一种基于似然比的信号检测方法。

假设 z 为观测像元 $\boldsymbol{r}$ 到分类器 q^{T} 的投影结果。基于 z 的信号检测模型可以用如下两个假设来表示：

$$\begin{aligned} H_0 &: z=q^{\mathrm{T}}\boldsymbol{n}\cong p_o(z)\\ H_1 &: z=\alpha_p+q^{\mathrm{T}}\boldsymbol{n}\cong p_1(z)\end{aligned} \tag{23}$$

其中原假设 H_0 表示目标信号 α_p 不存在，即只存在噪声(估计噪声)，对立假设 H_1 表示 α_p 存在。

与式(23)相应的 N-P 检测器表示如下：

$$\delta_{NP}(z)=\begin{cases}1, & z=q^{\mathrm{T}}\boldsymbol{n}\geqslant\tau\\ 0, & z=q^{\mathrm{T}}\boldsymbol{n}<\tau\end{cases} \tag{24}$$

式(24)表示当 $z\geqslant\tau$ 时，H_0 为真；当 $z<\tau$ 时，H_1 为真；τ 为阈值。

定义虚警概率 P_F 和检测概率 P_D 如下：

$$P_F=\int_{\tau}^{\infty}p_0(z)\mathrm{d}z \tag{25}$$

$$P_D=\int_{\tau}^{\infty}p_1(z)\mathrm{d}z \tag{26}$$

式(26)中 P_D 表示 N-P 检测器对真实目标信号 α_p 的检测能力。因此，P_D 值越高，估计误差越小，检测器性能越好。

4.2 SSP 的检测概率和虚警概率

用式(5)的 $\tilde{\boldsymbol{q}}_{\mathrm{SSP}}^{\mathrm{T}}$ 替代式(23)中的 q^{T}，则混合像元目标检测模型可表示如下：

$$\begin{aligned} H_0 &: z=\tilde{\boldsymbol{q}}_{\mathrm{SSP}}^{\mathrm{T}}\boldsymbol{n}=\hat{n}_{\mathrm{SSP}}\cong p_o(z)\\ H_1 &: z=\alpha_p+\hat{n}_{\mathrm{SSP}}\cong p_1(z)\end{aligned} \tag{27}$$

式中 $\hat{n}_{\mathrm{SSP}}$ 表示 SSP 估计的误差，H_0 表示混合像元中不存在目标信号 $\boldsymbol{d}$，H_1 表示混合像元中存在目标信号 $\boldsymbol{d}$。

根据式(7)和式(27)，可得 SSP 的误差协方差矩阵 $\boldsymbol{\Sigma}_{\mathrm{SSP}}$ 如下：

$$\boldsymbol{\Sigma}_{\mathrm{SSP}}=E\left[\varepsilon_{\mathrm{SSP}}\varepsilon_{\mathrm{SSP}}^{\mathrm{T}}\right]=E\left[\hat{n}_{\mathrm{SSP}}\hat{n}_{\mathrm{SSP}}^{\mathrm{T}}\right]=\sigma^2\frac{\boldsymbol{d}^{\mathrm{T}}\boldsymbol{P}_U^{\perp}\boldsymbol{P}_M\boldsymbol{P}_M\boldsymbol{P}_U^{\perp}\boldsymbol{d}}{\boldsymbol{d}^{\mathrm{T}}\boldsymbol{P}_U^{\perp}\boldsymbol{d}\boldsymbol{d}^{\mathrm{T}}\boldsymbol{P}_U^{\perp}\boldsymbol{d}}=\frac{\sigma^2}{\boldsymbol{d}^{\mathrm{T}}\boldsymbol{P}_U^{\perp}\boldsymbol{d}} \tag{28}$$

假设随机噪声 $\boldsymbol{n}$ 为零均值的高斯白噪声，且协方差矩阵为 $\sigma^2\boldsymbol{I}$。用式(28)代入式(27)得

$$\begin{aligned} p_o(z) &\approx N(0,\sigma^2(\boldsymbol{d}^{\mathrm{T}}\boldsymbol{P}_U^{\perp}\boldsymbol{d})^{-1})\\ p_1(z) &\approx N(\alpha_p,\sigma^2(\boldsymbol{d}^{\mathrm{T}}\boldsymbol{P}_U^{\perp}\boldsymbol{d})^{-1})\end{aligned} \tag{29}$$

因此可得 SSP 的 N-P 检测器阈值 τ_{SSP} 如下：

$$\tau_{\mathrm{SSP}}=\sigma(\boldsymbol{d}^{\mathrm{T}}\boldsymbol{P}_U^{\perp}\boldsymbol{d})^{-1/2}\Phi^{-1}(1-P_F) \tag{30}$$

式中 $\Phi(x)$ 为标准正态分布变量的积分函数，$\Phi^{-1}(x)$ 为 $\Phi(x)$ 的反函数，

$$\Phi(x)=\int_{-\infty}^{x}\frac{1}{\sqrt{2\pi}}\mathrm{e}^{-\frac{t^2}{2}}\mathrm{d}t \tag{31}$$

由式(30)可得 SSP 的检测概率 P_{D_SSP} 如下：

$$P_{D\_\mathrm{SSP}}=1-\Phi\left(\Phi^{-1}(1-P_F)-\frac{\alpha_p}{\sigma(\boldsymbol{d}^{\mathrm{T}}\boldsymbol{P}_U^{\perp}\boldsymbol{d})^{-1/2}}\right)=1-\Phi\left(\Phi^{-1}(1-P_F)-\sqrt{SNR_{\mathrm{SSP,max}}}\right) \tag{32}$$

式(32)表示 P_{D_SSP} 为 $\boldsymbol{d}^{\mathrm{T}}\boldsymbol{P}_U^{\perp}\boldsymbol{d}$ 的表达式，其表示 $\boldsymbol{d}$ 投影到背景补空间 $\langle\boldsymbol{U}^{\perp}\rangle$ 值的度量。投影值越大，$\boldsymbol{d}$ 与 $\boldsymbol{U}$ 的相似性越小，检测性能越好。另外，式(32)还表示 P_{D_SSP} 由信噪比 SNR 度量，信噪比越大，检测概率越大。

4.3 KSSP 的检测概率和虚警概率

用式(11)中的 $\tilde{\boldsymbol{q}}_{\mathrm{SSP}\phi}^{\mathrm{T}}$ 替代式(23)中的 q^{T}，则混合

像元目标检测模型可表示如下:

$$H_0: z=\tilde{\boldsymbol{q}}_{\mathrm{SSP}\phi}^{\mathrm{T}}\boldsymbol{n}=\hat{n}_{\mathrm{SSP}\phi}\cong p_0(z)$$
$$H_1: z=\alpha_p+\hat{n}_{\mathrm{SSP}\phi}\cong p_1(z) \tag{33}$$

式中 $\hat{n}_{\mathrm{SSP}\phi}$ 表示特征空间 SSP 估计的误差。

根据式(13)和式(33), 可得特征空间中 SSP 的误差协方差矩阵 $\boldsymbol{\Sigma}_{\mathrm{SSP}\phi}$ 如下:

$$\boldsymbol{\Sigma}_{\mathrm{SSP}\phi}=E\left[\boldsymbol{\varepsilon}_{\mathrm{SSP}\phi}\boldsymbol{\varepsilon}_{\mathrm{SSP}\phi}^{\mathrm{T}}\right]=E\left[\hat{\boldsymbol{n}}_{\mathrm{SSP}\phi}\hat{\boldsymbol{n}}_{\mathrm{SSP}\phi}^{\mathrm{T}}\right]=\frac{\theta^2}{k_{dd}-\boldsymbol{K}_{dU}\boldsymbol{A}_\phi\boldsymbol{\Sigma}_\phi^{-1}\boldsymbol{A}_\phi^{\mathrm{T}}\boldsymbol{K}_{Ud}} \tag{34}$$

假设随机噪声 $\boldsymbol{n}_\phi$为零均值的高斯白噪声, 且协方差矩阵为$\boldsymbol{\theta}^2\boldsymbol{I}$。用式(34)代入式(33)得

$$p_o(z)\approx N(0,\theta^2(k_{dd}-\boldsymbol{K}_{dU}\boldsymbol{A}_\phi\boldsymbol{\Sigma}_\phi^{-1}\boldsymbol{A}_\phi^{\mathrm{T}}\boldsymbol{K}_{Ud})^{-1})$$
$$p_1(z)\approx N(\alpha_p,\theta^2(k_{dd}-\boldsymbol{K}_{dU}\boldsymbol{A}_\phi\boldsymbol{\Sigma}_\phi^{-1}\boldsymbol{A}_\phi^{\mathrm{T}}\boldsymbol{K}_{Ud})^{-1}) \tag{35}$$

由此可得 KSSP 的 N-P 检测器阈值 τ_{KSSP} 如下:

$$\tau_{\mathrm{KSSP}}=\theta\times\frac{\Phi^{-1}(1-P_F)}{(k_{dd}-\boldsymbol{K}_{dU}\boldsymbol{A}_\phi\boldsymbol{\Sigma}_\phi^{-1}\boldsymbol{A}_\phi^{\mathrm{T}}\boldsymbol{K}_{Ud})^{1/2}} \tag{36}$$

由式(36)得 KSSP 的检测概率 P_{D_KSSP} 如下:

$$P_{D\_\mathrm{KSSP}}=1-\Phi\left(\Phi^{-1}(1-P_F)-\frac{\alpha_p}{\theta(k_{dd}-\boldsymbol{K}_{dU}\boldsymbol{A}_\phi\boldsymbol{\Sigma}_\phi^{-1}\boldsymbol{A}_\phi^{\mathrm{T}}\boldsymbol{K}_{Ud})^{-1/2}}\right)=1-\Phi\left(\Phi^{-1}(1-P_F)-\sqrt{SNR_{\mathrm{SSP}\phi,\max}}\right) \tag{37}$$

式(37)表示 P_{D_KSSP} 为 $\phi(\boldsymbol{d})^{\mathrm{T}}\boldsymbol{P}_{U\phi}^{\perp}\phi(\boldsymbol{d})$ 的表达式, 其表示在特征空间中 $\boldsymbol{d}$ 投影到背景补空间$\langle\boldsymbol{U}^{\perp}\rangle$值的度量, 投影值越大, 表示特征空间中 $\boldsymbol{d}$ 与 $\boldsymbol{U}$ 的相似性越小, 检测性能越好。另外, 式(37)还表示 P_{D_KSSP} 由 *SNR* 度量, 信噪比越大, 检测概率越大。

5 实验结果

实验所用数据分别为 USGS(Clark, 2007)数字光谱数据库模拟的高光谱混合像元数据和 HYDICE 采集到的城市高光谱数据集(Pazak,2009)。

5.1 模拟高光谱数据实验

首先, 从 USGS 数字光谱数据库中选择 3 个纯物质光谱, 分别为光卤石、铵明矾石、黑云母(光谱曲线如图 2)作为端元光谱, 且本实验选择黑云母为待检测的目标。这 3 种光谱都是波段数为 224 维的数据。再根据 Hapke 数据模拟过程(吴波等, 2006)合成非线性的高光谱混合像元数据, 最后对合成的数据做如下实验。为了充分证明 KSSP 对亚像元目标检测的有效性, 用两种不同分布产生的丰度矩阵 $\boldsymbol{a}$, 再根据 Hapke 模型生成了两个像元数为 50 的模拟数据集, 且每个数据集的入射角为 30°、*SNR* 为 30, 最后对这两个数据集用多项式核函数进行仿真。

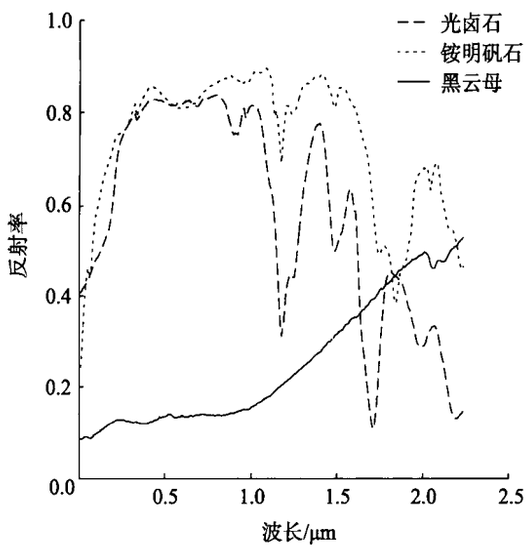

图 2 光卤石、铵明矾石、黑云母的光谱反射值曲线

数据集 1: Dirichlet 分布(Nascimento, 2005)

丰度矩阵 $\boldsymbol{a}$ 为按 Dirichlet 分布的随机生成的混合像元丰度矩阵。

数据集 2: 小概率目标分布

合成的 50 个模拟混合像元中的 3 种端元的比份即其丰度矩阵 $\boldsymbol{a}$ 如表 1 所示。

表 1 数据集 2 中各端元的丰度分布

	1—19	20	21	…	29	30—50
光卤石	0.5	0.45	0.455	…	0.495	0.5
铵明矾石	0.5	0.45	0.455	…	0.495	0.5
黑云母	0	0.1	0.09	…	0.01	0

由于实验中合成的非线性混合像元的丰度是已知的, 因此, 我们把 SSP 和本文提出的 KSSP 检测到的目标丰度与真实丰度用相似度 COR(陶雪涛等, 2008), 丰度角 AAD(Miao, *et al.*, 2007)和均方根误差 RMSE 3 种指标分别做比较, 来评价算法性能。除此之外, 根据第 4 节描述的 ROC 曲线进一步评价两种算法的检测性能。

通过多次实验确定, 数据集 1 实验中, KSSP 核参数分别为 a=0.001, b=0.2, c= –0.01。数据集 2 实验中, KSSP 核参数分别为 a=0.1, b=0.01, c=0.8。数据集 1 与数据集 2 的目标检测的结果曲线如图 3(a)(b)所示。表 2 和表 3 中分别列出了 SSP、KSSP 算法对数据集 1 和数据集 2 分别检测出的目标丰度与真实丰度之间基于上述 3 种指标的性能比较结果。图 4 为两数据集的 *SNR* 都为 30 的情况下 SSP 与 KSSP 检测器的 ROC 曲线图。

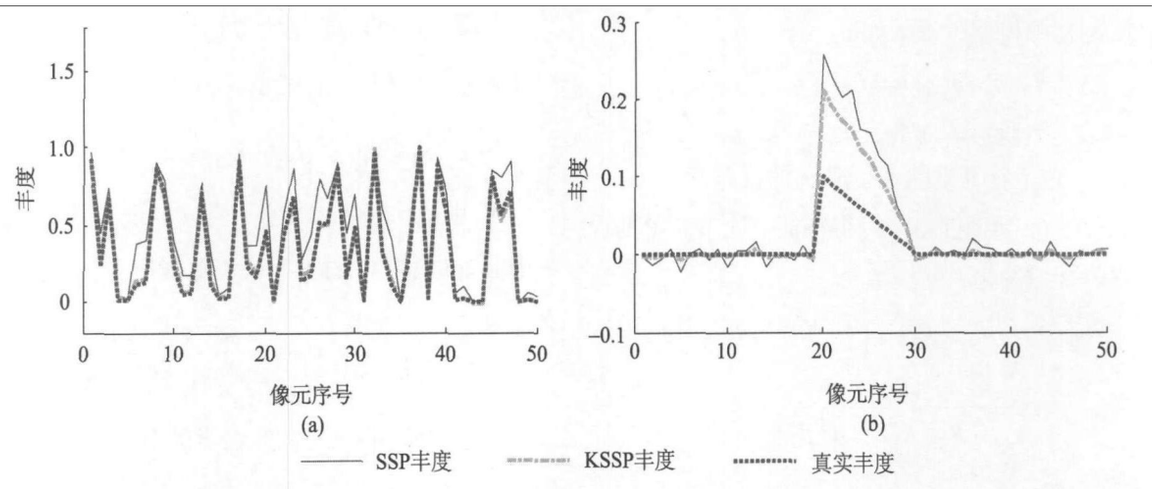

图 3 SSP、KSSP 检测的目标结果与真实丰度的曲线比较图

(a) 数据集 1; (b) 数据集 2

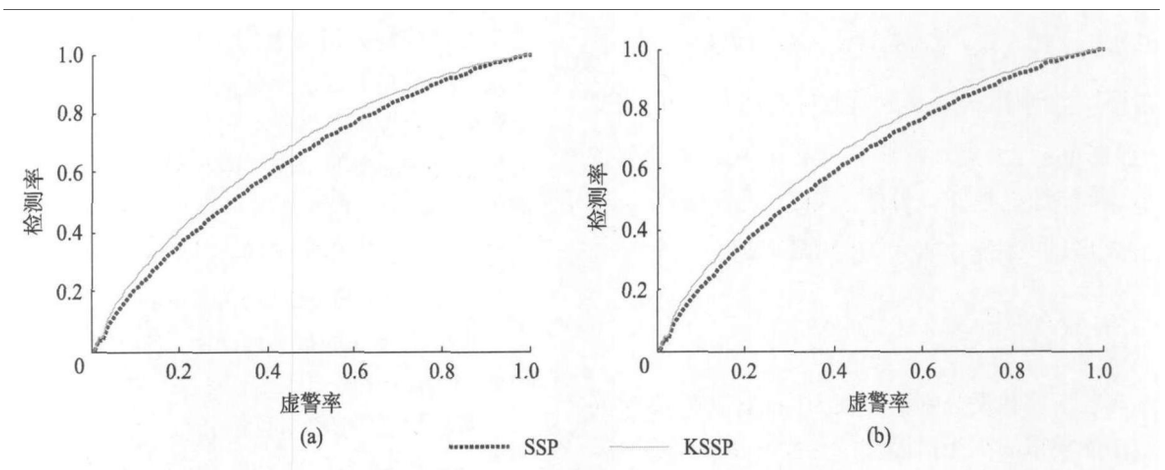

图 4 SSP 与 KSSP 检测器的 ROC 曲线图

(a) 数据集 1; (b) 数据集 2

通过曲线比较图(图 3)可以看出 KSSP 得到的结果与真实丰度十分相近，且结果还显示出 KSSP 方法对噪声有明显的抑制作用。表 2 与表 3 中的性能指标比较说明 KSSP3 个性能指标均优于 SSP，且图 4 进一步说明 KSSP 的检测性能优于 SSP。

表2 SSP、KSSP对数据集1的目标丰度检测结果与真实丰度之间基于相似度、丰度角和均方根误差指标的性能比较

	相关系数	丰度角	均方根误差
SSP	0.957691	0.231915	0.153329
KSSP	0.998236	0.0459696	0.0223425

表3 SSP、KSSP对数据集2的目标丰度检测结果与真实丰度之间基于相似度、丰度角和均方根误差指标的性能比较

	相关系数	丰度角	均方根误差
SSP	0.986418	0.151409	0.0487654
KSSP	0.996017	0.081963	0.0338377

5.2 真实图像实验

该部分实验数据为 HYDICE 采集到的城市高光谱数据集(图 5)，大小为 307×307 像元，其包含 210 个波段。为了提高算法的性能，我们去除低信噪比

图 5 城市高光谱数据集(波段 50)

和水蒸气吸收波段(1—4, 76, 87, 101—111, 136—153 和 198—210)后剩余 162 个波段用于本实验。城市高光谱数据集采集的区域包含人工目标、森林地带及它们的混合: 沥青、屋顶、草地和树木。由于光谱的可变性, 在实验之前首先通过手工方式从高光谱数据中选取参考的端元光谱, 本实验选择图中坐标[197, 62]、[213, 124]、[87, 134]及[31, 274]分别作为沥青、屋顶、草地及树木的参考光谱。

选择 RBF 核作为 KSSP 核函数且实验证明 KSSP 的 RBF 核参数 $2\sigma^2$ 选在 2 到 5 之间均可。图 6 中的 KSSP 的核参数 $2\sigma^2$=4。图 6 为 SSP 算法分别对沥青、屋顶、草地和树木 4 种目标的检测结果。图 7 为 KSSP 算法分别对上述 4 种目标的检测结果。图 6、图 7 中子图(a)、(b)、(c)、(d)分别表示沥青、屋顶、草地、树木的检测结果。图中纯黑色像元表示该目标在该像元所占比重为 0, 而纯白色表示比重为 1。从图中可以看出, KSSP 算法把每个目标都检测出来了, 但 SSP 检测出的结果比较模糊。

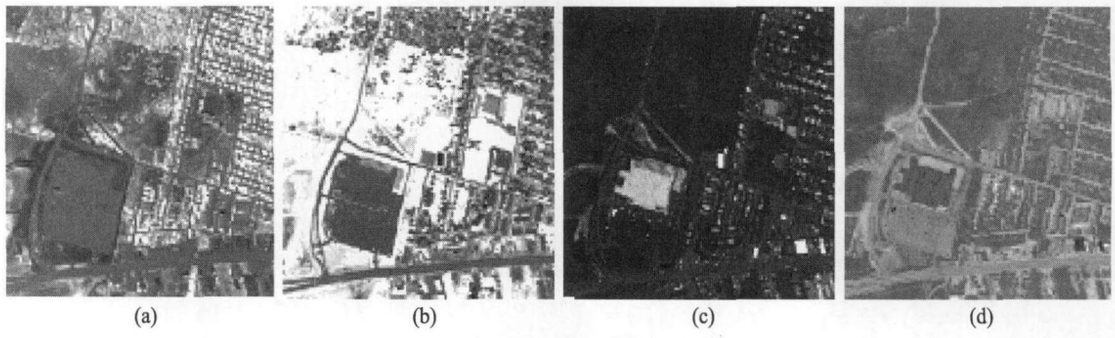

图 6 SSP 对城市高光谱数据图像中 4 种目标的检测结果
(a) 沥青; (b) 屋顶; (c) 草地; (d) 树木

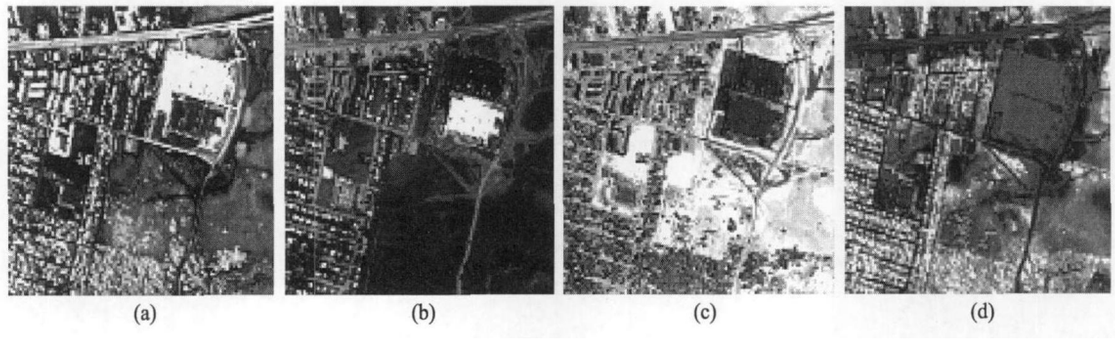

图 7 KSSP 对城市高光谱数据图像中 4 种目标的检测结果
(a) 沥青; (b) 屋顶; (c) 草地; (d) 树木

6 结 论

提出了一种核信号空间正交投影(KSSP)的目标检测方法。该方法运用核技巧将混合像元矢量经非线性映射函数从原始(低维)空间转换到特征空间(高维), 使得像元在特征空间中满足线性混合, 然后在特征空间中运用基于线性混合模型的 SSP 检测信号。KSSP 运用核函数方法既避免了非线性映射函数的计算, 又保留了非线性分解精度较高的优点。实验证明 KSSP 的检测性能优于 SSP, 且 KSSP 明显地抑制了噪声。

REFERENCES

Bian Z Q and Zhang X G. 2000. Pattern Recognition. Beijing: Tsinghua University Press: 224–226

Chang C I, Zhao X L, Althouse M L G, and Pan J J. 1998. Least squares subspace projection approach to mixed pixel classification for hyperspectral images. *IEEE Transactions on Geoscience and Remote Sensing*, **36**(3): 898–912

Capobianco L and Camps-Valls G. 2008. Target detection with a contextual kernel orthogonal subspace projection. Image and Signal Processing for Remote Sensing XIV, SPIE Digital Library, Cardiff, UK

Clark R N. 2007. Spectral Library 06. USGS Digital Spectral Libraries[DB/OL]. [2009-05-10]. http://speclab.cr.usgs.gov

Jia S. 2007. Unsupervised hyperspectral unmxiing Theory and Techniques. Hangzhou, Zhejiang University: 69

Kwon H and Nasrabadi N M. 2005. Kernel orthogonal subspace projection for hyperspectral signal classification. *IEEE Transcactions on Geoscience and Remote Sensing*, **43**(12): 2952–2962

Miao L D and Qi H R. 2007. Endmember extraction from highly mixed data using minimum volume constrained nonnegative matrix factorization. *IEEE Transactions on Geoscience and Remote Sensing*, **45**(3): 765–777

Nascimento J M P and Dias J M B. 2005. Vertex component analysis: a fast algorithm to unmix hyperspectral data. *IEEE Transactions on Geoscience and Remote Sensing*, **43**(4): 898–910

Pazak R. 2009. Hypercube. URBAIN.zip [EB/OL]. [2009-08-02]. http:// www. tec.army.mil/ Hypercube

Shawe-Taylor J and Cristianini N. 2005. Kernel methods for pattern analysis. Beijing: China machine press: 20–42

Tong Q X, Zhang B and Zheng L F. 2006. Hyperspectral Remote Sensing. Beijing: Higher Education Press: 255–262

Tao X T, Wang B and Zhang L M. 2008. New scheme for decomposition of mixed pixels of remote sensing images based on nonnegative matrix factorization. *Information and Electronic Engineering*, **6**(1): 34–39

Wu B, Zhang L P and Li P X. 2006. Unmixing hyperspectral imagery based on support vector nonlinear approximating regression. *Journal of Remote Sensing*, **10**(3): 312–318

附中文参考文献

边肇棋, 张学工. 2000. 模式识别. 北京: 清华大学出版社: 224–226

贾森. 2007. 非监督的高光谱图像解混技术研究. 杭州: 浙江大学学位论文: 69

童庆禧, 张兵, 郑兰芬. 2006. 高光谱遥感: 原理、技术与应用. 北京: 高等教育出版社: 255–262

陶雪涛, 王斌, 张立明. 2008. 基于 NMF 的遥感图像混合像元分解新方法. 信息与电子工程, **6**(1): 34–39

吴波, 张良培, 李平湘. 2006. 基于支撑向量回归的高光谱混合像元非线性分解. 遥感学报, **10**(3): 312–318